IEEE Access
Multidisciplinary | Rapid Review | Open Access Journal

Received January 14, 2018, accepted January 22, 2018, date of publication January 26, 2018, date of current version March 12, 2018.

Digital Object Identifier 10.1109/ACCESS.2018.2799145

Versatile Locomotion Control of a Hexapod Robot Using a Hierarchical Network of Nonlinear Oscillator Circuits

LUDOVICO MINATI[1,2], (Senior Member, IEEE), MATTIA FRASCA[3], (Senior Member, IEEE), NATSUE YOSHIMURA[4], AND YASUHARU KOIKE[4]

[1]Tokyo Tech World Research Hub Initiative, Institute of Innovative Research, Tokyo Institute of Technology, Yokohama 226-8503, Japan
[2]Complex Systems Theory Department, Institute of Nuclear Physics, Polish Academy of Sciences, 31-342 Kraków, Poland
[3]Department of Electrical Electronic and Computer Engineering, University of Catania, 95125 Catania, Italy
[4]FIRST, Institute of Innovative Research, Tokyo Institute of Technology, Yokohama 226-8503, Japan

Corresponding author: Ludovico Minati (lminati@ieee.org)

This work was supported in part by JSPS under Grant KAKENHI 26112004 and Grant KAKENHI 17H05903 and in part by the Center of Innovation Program from the Japan Science and Technology Agency.

ABSTRACT A novel hierarchical network based on coupled nonlinear oscillators is proposed for motor pattern generation in hexapod robots. Its architecture consists of a central pattern generator (CPG), producing the global leg coordination pattern, coupled with six local pattern generators, each devoted to generating the trajectory of one leg. Every node comprises a simple nonlinear oscillator and is well-suited for implementation in a standard field-programmable analog array device. The network enables versatile locomotion control based on five high-level parameters which determine the inter-oscillator coupling pattern via simple rules. The controller was realized on dedicated hardware, deployed to control an ant-like hexapod robot, and multi-sensory telemetry was performed. As a function of a single parameter, it was able to stably reproduce the canonical gaits observed in six-legged insects, namely the wave, tetrapod, and tripod gaits. A second parameter enabled driving the robot in ant-like and cockroach-like postures. Three further parameters enabled inhibiting and resuming walking, steering, and producing uncoordinated movement. Emergent phenomena were observed in the form of a multitude of intermediate gaits and of hysteresis and metastability close to a point of gait transition. The primary contributions of this paper reside in the hierarchical controller architecture and associated approach for collapsing a large set of low-level parameters, stemming from the complex hexapod kinematics, into only five high-level parameters. Such parameters can be changed dynamically, an aspect of broad practical relevance opening new avenues for driving hexapod robots via afferent signals from other circuits representing higher brain areas, or by means of suitable brain-computer interfaces. An additional contribution is the detailed characterization via telemetry of the physical robot, involving the definition of parameters which may aid future comparison with other controllers. The present results renew interest into analog CPG architectures and reinforce the generality of the connectionist approach.

INDEX TERMS Analog locomotion control, bio-inspired control, central pattern generator (CPG), field-programmable analog array (FPAA), hexapod robot, hierarchical network, locomotion gait, non-linear oscillator, synchronization.

I. INTRODUCTION

A. WALKING ROBOTS

Walking robots are of interest from both application and research perspectives: on one hand, they offer unsurpassed resilience and maneuverability over irregular terrains, reaching places inaccessible to rovers, and on the other they yield important insights into animal behavior and neurophysiology, since many species possess four or more legs, and adaptive motor control is arguably among the most important functions supporting survival [1]–[4]. Yet, their viability remains constrained by the complexity inherent in controlling their locomotion, a task that has stimulated and continues to

stimulate research aiming to develop circuit-based as opposed to purely algorithmic controllers. The purpose of efforts in this area is not only to replicate electronically the biological neural architectures which solve the locomotion control problem for a variety of structures across diverse scales (e.g., from micro-insects to large mammals), but also to practically realize high levels of flexibility and adaptability (e.g. responding to unpredictable stimuli, failures etc.) which can only be attained with recourse to emergent phenomena, about the induction and management of which still little is known [5]–[8].

B. ARTIFICIAL CENTRAL PATTERN GENERATORS

Analog circuit-based approaches to walking robot control are often inspired by the highly influential neurobiological discovery of *Central Pattern Generators* (CPGs). These are pervasive architectures which intrinsically generate periodic oscillations, and drive the leg joints via other downstream neural structures. In most legged animals, CPGs are capable of creating a multitude of stereotyped gaits, i.e. regular phase relationships between leg movements, such as walking and trotting, adapted to support diverse essential behaviors such as foraging and fleeing over highly heterogeneous surfaces. As consistently indicated by lesion studies, the generation of rhythmic patterns occurs spontaneously without need for any external input; however, biological CPGs invariably receive afferences from other ganglia or higher brain regions, which influence motion initiation and inhibition, and determine the gait that is generated alongside its frequency and other parameters. In particular, CPG activity can often be externally modulated to produce slow drifts in gait or sudden, discrete movements, though the exact mechanisms underlying the latter remain incompletely understood [9]–[12].

A rich literature on implementing artificial CPGs in the form of electronic circuits is available [4], [8], [12], [13]. While reviewing it is beyond the scope of the present study, we shall mention that three broad approaches based on nonlinear dynamical systems have been considered: 1) circuits predicated upon physiologically-realistic models of spiking and bursting neurons [14], [15]; 2) circuits encompassing lower-order coupled oscillators with isolated periodic dynamics, which although biologically less plausible often yield a more compact representation having similar emergent properties [4], [16]–[21]; 3) circuits involving chaos control, wherein interaction with the environment stabilizes the oscillation of one or more chaotic oscillators into a periodic orbit, and as a function of one or more parameters such orbit can be altered to yield distinct gaits [22], [23].

We note that in circuits of coupled oscillators the gait properties can oftentimes be influenced via two separate routes: 1) acting on one or more internal parameters of each oscillator (i.e., of the Hopf, Matsuoka, van der Pol or Kuramoto oscillators as in [16]–[18]), or 2) changing the topology and strengths of the connections coupling the oscillators, such as in [4] and [19]–[21]. We refer to the latter as the *connectionist approach*.

Besides investigations in which the robot and environment were both simulated, also a considerable fraction of experimental studies, wherein the robot was physically realized, have resorted to numerical implementation of CPG circuits, as this minimizes the engineering challenges associated with building the circuit and adjusting its structure and parameters to obtain the desired behaviors. However, there is inherent value in implementing CPGs by means of analog electronic circuits: not only this usually results in much smaller and lower-power systems, but there are also a multitude of aspects which can have a profound impact on global emergent properties in systems of synchronized non-linear elements. These, in particular, include the stability of numerical solutions, the effects of discretization and noise, as well as non-ideal behaviors, which are not trivial to capture numerically, and the parametric mismatches making the constituent elements non-identical [20], [24]–[26].

Early physical realizations of CPG circuits were based on off-the-shelf components such as operational amplifiers, yielding lowest cost but also largest size and lowest flexibility [19], [20]. Much work has since been done on implementations involving ad-hoc designed CMOS ICs, substantially reducing size and opening the way to increased flexibility through allowing seamless reconfiguration of connections and alteration of oscillator parameters via pass-gates and switched-capacitor circuits [13], [27]. Custom CMOS ICs have enabled, for example, the compact implementation of spiking neural models [15] as well as of a multitude of nonlinear oscillators and cellular neural networks [4], [21]. Such devices are, however, still relatively inflexible, because it is difficult to exert control over large numbers of parameters without developing prohibitively complex configuration logic. This represents an important limitation, since for research as well as practical applications one often requires a high level of flexibility in controlling the global pattern generation and even the operation of individual legs. Furthermore, the availability of custom ICs is by definition limited to the centers where they are developed and collaborating institutions, hampering the replication of studies.

Recently, some *Field Programmable Gate Array* (FPGA)-based implementations of CPG circuits have also been reported; although notable in terms of size and power, conceptually they are equivalent to numerical simulations on standard computers and as such share the same limitations [28]. By contrast, *Field-Programmable Analog Arrays* (FPAAs) are switched-capacitor systems which architecturally resemble programmable logic devices (PLDs), but implement analog rather than digital circuitry, and enable the rapid physical deployment of near-arbitrary circuits based on only few commercially-available, general-purpose arrays. Representative devices include a multitude of arrays of interconnected and configurable analog blocks, each of which comprises 1) a set of operational amplifiers, 2) a set of capacitors having diverse values, 3) switch matrices allowing the realization of almost any combination of connections between the amplifiers and the capacitors, 4) one

or more banks of static memory adapted to store a bit-string representing the current configuration and 5) means for externally uploading new configurations without disrupting operation [29]–[32]. Countless non-linear oscillators have been realized using this technology (see [33] for a review), and a recent study has introduced a circuit conjugating a rich dynamical repertoire with compactness [26]. However, to the authors' knowledge an FPAA-based CPG implementation is missing to date.

C. SCOPE AND STRUCTURE OF THIS STUDY

In this work, a versatile controller for a hexapod robot was developed and experimentally realized in the form of a hierarchical network of coupled oscillators controlled by five high-level parameters $P_1 \ldots P_5$. As detailed below, in this initial study these parameters are kept static, i.e. are set once before each experimental run, but in the future they will be controlled dynamically, i.e. as $P_1(t) \ldots P_5(t)$, for example based on circuits representing higher brain areas or input from brain-computer interfaces.

A preliminary evaluation of the controller was performed based on a physically-realized hexapod robot, and a range of kinematic measurements are presented to illustrate its capabilities. Suitability for efficient implementation in FPAAs was a key factor driving the design of the proposed controller, with the aim of overcoming many of the above-mentioned limitations associated to realizations based on custom ICs (i.e., availability and reconfigurability) or FPGAs (i.e., digital vs. analog implementation). Though the proposed FPAA-based CPG realization could in principle be generalized to driving diverse robot types (e.g. bipeds, quadrupeds, even swimming robots), here the focus is restricted to developing a specific controller for hexapod robots.

The approach is predominantly a connectionist one, wherein according to simple mapping laws, the five high-level control parameters $P_1 \ldots P_5$ influence the strengths of a large number of links (realized as input gains), realizing a considerable level of flexibility in terms of gait pattern, level of coordination, posture and steering control. A hierarchical approach, inspired by the architecture of biological CPGs, was applied to realize a control system having at its core a network of six oscillators, each one corresponding to a leg of the robot and coupled through downstream unidirectional connections to a separate (i.e., local) pattern generator individually driving the joints of the associated leg.

The topology of the circuit instanced at each node can be viewed as a ring oscillator onto which two integrators are overlaid; saturation at the outputs of latter represents the main type of non-linearity in the system. In a previous study, coupling such oscillators revealed non-trivial phenomena including a form of ''remote synchronization'', wherein amplitude fluctuations become entrained between non structurally-adjacent nodes, leading to the emergence of small-world synchronization topology from underlying structural connectivity arranged as an elementary ring network [26]. The possibility of easily building coupled configurations encompassing more than one unit and of exploring large regions in the multidimensional space of the parameters of the system, is fundamental to the present work: it provides the substrate for controller versatility, which is practically realized, as mentioned above, by mapping five high-level control parameters onto a large number of gains (connection strengths) across the two layers of the hierarchical controller.

This work aims to provide the following contributions with respect to the existing literature. First, we address the issues of flexibility and availability associated with CPGs deployed in custom ICs, and demonstrate the possibility for seamlessly reconfigurable implementation in FPAAs. Second, we introduce a pure hierarchical approach where robot motion is controlled by a CPG which downstream drives independent local pattern generators (LPGs) instanced for each leg, and demonstrate that this approach confers a high level of flexibility in gait, posture and coordination. Third, we demonstrate a means of dealing with the large number of low-level parameters inherent in specifying one CPG and six independent LPGs: by superimposing a minimal number of canonical gaits and postures, it is possible to collapse them into as few as five high-level parameters, which specify in a continuous manner which configurations are active at a given time. Fourth, we report on a comprehensive experimental characterization involving telemetry of a physical robot, and the calculation of measures which also warrant future consideration as means for comparing controllers in this area.

The remainder of this paper is organized as follows. In Sec. II the controller network is introduced and its design and dynamics are illustrated. In Sec. III the hexapod robot design and the experimental results obtained driving it with the proposed controller are described. Finally, in Sec. IV the main features of the proposed approach are discussed with reference to other known controllers.

II. CONTROLLER NETWORK

A. ARCHITECTURE

1) HIERARCHICAL NETWORK

As mentioned in the previous section, the proposed controller consists of two hierarchical levels: at the top, one CPG, and at the bottom, six LPG structures, one per leg (Fig. 1). The CPG operates spontaneously, in other words it does not receive any external afferences and is instead controlled by five high-level parameters. Since the focus in this initial study was on motor pattern generation, the parameters are set once and kept static (i.e., constant) during each experimental run. As illustrated in greater detail below, they control gait selection (P_1), walking initiation and inhibition (P_2), strength of coupling between the CPG and the LPGs (P_3), posture (P_4) and steering (P_5); a summary is provided in Table 1.

The CPG provides the overall pattern, i.e. determines the phase relationships between the leg swing and stand cycles.

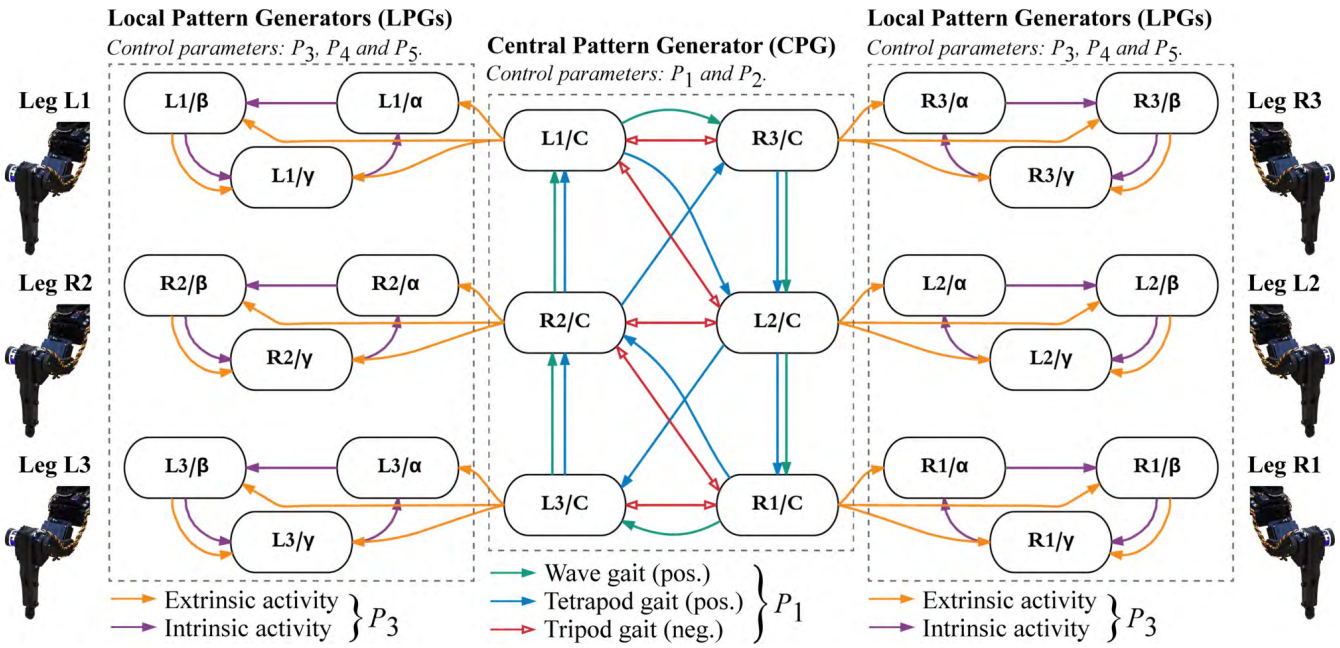

FIGURE 1. **Hierarchical controller design. Overall network architecture, delineating a central pattern generator (CPG, 6 nodes) and six local pattern generators (LPGs, 3 nodes each). Each leg is associated to one CPG node (e.g., node L1/C) driving a corresponding LPG (e.g., nodes L1/α, L1/β and L1/γ), which in turn drives a leg (note: figure layout not corresponding to physical leg layout). The link strengths among the CPG nodes depend on the gait selection parameter P_1 and on the activation parameter P_2, and the link strengths within each LPG depend on the coupling strength parameter P_3 and on the posture parameter P_4. Different colors highlight which links have increased intensity for a given gait (CPG) or configuration (LPGs); the full relationships between parameters and connections are specified in Tables 2, 4 and 6.**

TABLE 1. **Summary of the high-level control parameters $P_1 \ldots P_5$. In this initial study they are set once before each experimental run and kept static thereafter, but in future work these can be changed dynamically as $P_1(t) \ldots P_5(t)$ to drive the robot purposefully. CPG: Central Pattern Generator. LPGs: Local Pattern Generators.**

Parameter	Range	Target	Denomination	Function
P_1	$[0, 1]$	CPG	Gait selection parameter	Determines the phase relationships between legs, e.g. allows choosing between wave (slow), tetrapod (metachronal, medium speed) and tripod (fast) gaits
P_2	$[-1, 1]$	CPG	Activation parameter	Allows inhibiting and approximately reversing the CPG activity, i.e. walking
P_3	$[0, 1]$	LPG	CPG → LPG coupling strength parameter	Determines the level of synchronization between the CPG and the LPGs (i.e., movement coordination)
P_4	$[0, 1]$	LPG	Posture parameter	Allows choosing between the ant-like and cockroach-like postures
P_5	$[-1, 1]$	LPG	Steering parameter	Allows steering the robot trajectory sideways

The CPG is unidirectionally coupled to the LPGs, which are independent of each other and receive no other input. They provide a flexible means of translating the signal generated by the CPG into three signals driving the joints of each leg, determining the precise trajectory of the coxa-body (α), tibia-femur (β) and femur-coxa (γ) joints during each cycle. Each LPG is internally wired as a ring, allowing it to potentially generate "intrinsic" sustained activity irrespective of "extrinsic" input from the associated CPG node, which is unsynchronized between legs due to unavoidable parametric mismatches (i.e., tolerances) between the physical oscillators (Fig. 1).

The proposed controller is specifically intended for driving hexapod robots with 18 degrees-of-freedom, a representative implementation of which is introduced in Sec. III for the sole purpose of experimentally confirming the viability of the controller. Throughout this paper, the six legs of a generic hexapod robot are denoted with L1, . . . , R3, where L/R stands for left/right, the leg pairs are numbered 1-3 from front to rear, and each leg has three degrees of freedom whose corresponding angles are referred to as α, β and γ.

Under the control of the proposed network, a hexapod robot can be made to walk in "ant-like" and "cockroach-like" postures; in the former, the power stroke is delivered using the coxa-body joint of all legs, whereas in the latter, the front and hind legs deliver the power stroke primarily using the tibia-femur joint. Regardless of the posture, locomotion can be attained by means of several gaits, including three "canonical" gaits. With this term, we refer to gaits which are highly conserved in insects, namely 1) the tripod gait, wherein two leg triplets, i.e. (L1,R2,L3) and (R1,L2,R3), conjointly alternate in their stance and swing phases, 2) the wave gait, characterized by the power stroke sequence L1, R2, L3, R1, L2, R3, and 3) the tetrapod or metachronal gait, wherein the power stroke sequence is (L1,R3), R2, (L3,R1), L2, i.e., the legs L1 and R3 and the legs L3 and R1 swing simultaneously. In insects, the wave, tetrapod and tripod gaits tend to be observed in conjunction with slow, medium and fast locomotion respectively [1], [2].

2) CENTRAL PATTERN GENERATOR (CPG)

The architecture of the CPG is predicated on the work of Arena and colleagues [4], [34], wherein the wave, tetrapod (metachronal) and tripod gaits were implemented in custom CMOS ICs applying the connectionist approach, that is by means of altering the coupling between oscillators while maintaining their internal parameters unaltered. The coupling schemes realizing these three gaits are taken directly from their work, however flipping link directions to account for the fact that the oscillator circuit chosen for implementation in this study, described below, has predominantly integrative dynamics and as such yields a phase lead rather than a lag or a delay.

The wave gait is implemented through six unidirectional positive connections having strength S_{L} and linking the following loop of nodes L1/C $\rightarrow$ R3/C $\rightarrow$ L2/C $\rightarrow$ R1/C $\rightarrow$ L3/C $\rightarrow$ R2/C $\rightarrow$ L1/C (green arrows in Fig. 1). The tetrapod (metachronal) gait is implemented through eight unidirectional positive connections having strength S_{M} or $S_{\mathrm{M}}/2$ and linking the following two intertwined loops of nodes: L1/C $\rightarrow$ L2/C $\rightarrow$ L3/C $\rightarrow$ R2/C $\rightarrow$ L1/C and R1/C $\rightarrow$ R2/C $\rightarrow$ R3/C $\rightarrow$ L2/C $\rightarrow$ R1/C (blue arrows in Fig. 1). The tripod gait is implemented through five bidirectional negative connections having strength $-S_{\mathrm{H}}$ or $-S_{\mathrm{H}}/2$ and linking the following ladder of nodes: L3/C $\leftrightarrow$ R1/C $\leftrightarrow$ R2/C $\leftrightarrow$ L2/C $\leftrightarrow$ L1/C $\leftrightarrow$ R3/C (red arrows in Fig. 1). The successful generation of the intended gait patterns based on the coupling schemes introduced in [4] and [34] despite profound differences in the oscillator circuit instanced at each node reinforces the generality of connectionist approach.

Extending the notion of continuous generalized gait introduced in [4] and [34], the CPG connection strengths are made to depend upon a single *gait selection parameter* $P_1 \in [0, 1]$. Namely, instead of having two separate mixing parameters, here a single high-level parameter akin to a speed setting, namely P_1, univocally sets the link strengths between all CPG nodes in such a manner as to realize the three canonical gaits. This is accomplished with recourse to the three sigmoidal membership functions $S_{\mathrm{L}}(P_1)$, $S_{\mathrm{M}}(P_1)$ and $S_{\mathrm{H}}(P_1)$, which reach unity respectively for $P_1 \approx 0$, $P_1 \approx 1/2$ and $P_1 \approx 1$:

$$\begin{cases} S_{\mathrm{L}}(P_1) = 1 - \dfrac{1}{1 + e^{A_{\mathrm{L}}(P_1 + C_{\mathrm{L}})}} \\ S_{\mathrm{M}}(P_1) = 1 - \dfrac{1}{1 + e^{A_{\mathrm{M}}(|P_1 + C_{\mathrm{M}}| + C_{\mathrm{M}}/2)}} \\ S_{\mathrm{H}}(P_1) = \dfrac{1}{1 + e^{A_{\mathrm{H}}(P_1 + C_{\mathrm{H}})}} \end{cases} \tag{1}$$

where empirically we set $A_{\mathrm{L}} = A_{\mathrm{M}} = A_{\mathrm{H}} = -20$, $C_{\mathrm{L}} = -0.3$ and $C_{\mathrm{M}} = C_{\mathrm{H}} = -0.5$; these settings, which are not critical, yield membership functions maximizing the responsiveness of the controller to parameter P_1 (Fig. 2), as ascertained in preliminary experiments not reported for brevity. In this manner, for $P_1 \approx 0$, $P_1 \approx 1/2$ and $P_1 \approx 1$ the canonical gaits are recovered, whereas other settings allow continuous transition between them via a multitude of "intermediate" gaits.

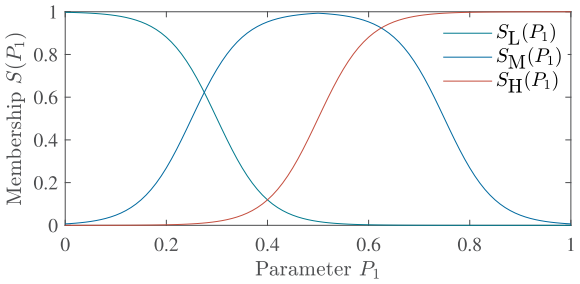

FIGURE 2. Membership functions for the wave gait $S_{\mathrm{L}}(P_1)$, tetrapod or metachronal gait $S_{\mathrm{M}}(P_1)$, and tripod gait $S_{\mathrm{H}}(P_1)$ as a function of gait selection parameter P_1.

As shown in Fig. 1, each CPG node is hardwired to receive input from up to three other CPG nodes, and linear superposition of the connections required for the three canonical gaits yields the continuous generalized gait. As detailed below, this is realized by acting on three parameters separately across all CPG nodes, namely gains G_1, G_2 and G_3.

The oscillator instanced at each CPG node and implemented in a corresponding FPAA device represents an adaptation of that described in [26]. Namely, the circuit consists of i) two gain and low-pass filtering stages which mix the inputs from other CPG nodes, yielding internal voltages v_1 and v_2, ii) a ring of three similar gain and low-pass filtering stages, yielding internal voltages v_3, v_4 and v_5, and iii) two integrators overlapped to the ring, yielding internal voltages v_6 and v_7 (Fig. 3a). In particular, each oscillator receives as input the voltages v_5 of three other oscillators, referred to as v_{A}, v_{B} and v_{C}, which are weighted by the input gains G_1, G_2 and G_3, respectively, mixed with the node's own output and fed into the ring as internal voltage v_2.[1] The available gait patterns are determined by the hardwired interconnections among inputs and outputs of the CPG nodes, and the specific gait generated at a given time is determined by the associated strengths (gains). The interconnection scheme realizing the graph in Fig. 1, alongside the corresponding gains, is specified in Table 2.

The system of ordinary differential equations corresponding to each CPG node can be written as follows:

$$\begin{cases} \dfrac{\mathrm{d}v_1}{\mathrm{d}t} = \Gamma\Big(2\pi F_1(G_1 v_{\mathrm{A}} + G_2 v_{\mathrm{B}} + G_3 v_{\mathrm{C}} - v_1), v_1\Big) \\ \dfrac{\mathrm{d}v_2}{\mathrm{d}t} = \Gamma\Big(2\pi F_2(G_4 v_1 + G_5 v_5 - v_2), v_2\Big) \\ \dfrac{\mathrm{d}v_3}{\mathrm{d}t} = \Gamma\Big(2\pi F_3(G_6 v_2 - v_3), v_3\Big) \\ \dfrac{\mathrm{d}v_4}{\mathrm{d}t} = \Gamma\Big(2\pi F_4(G_7 v_3 + G_8 v_6 - v_4), v_4\Big) \\ \dfrac{\mathrm{d}v_5}{\mathrm{d}t} = \Gamma\Big(2\pi F_5(G_9 v_4 + G_{10} v_7 - v_5), v_5\Big) \\ \dfrac{\mathrm{d}v_6}{\mathrm{d}t} = \Gamma\Big(K_1 v_2, v_6\Big) \\ \dfrac{\mathrm{d}v_7}{\mathrm{d}t} = \Gamma\Big(K_2 v_3, v_7\Big) \end{cases} \tag{2}$$

[1] We highlight that in the present implementation the factor of -0.8 introduced by the output gain stage is transparently taken into account when configuring the FPAAs to realize the prescribed coupling gains.

TABLE 2. Hardwired CPG node connectivity and corresponding weights (i.e., input gains), controlled by parameter P_1, which is a high-level setting as specified in Table 1. Voltages v_A, v_B and v_C denote the three inputs of each node (see Fig. 1), weighted respectively by the gains G_1, G_2 and G_3 (see Fig. 3), whereas voltages v_5 correspond to the node outputs. For brevity, S_H, S_M and S_L stand for $S_H(P_1)$, $S_M(P_1)$ and $S_L(P_1)$ according to Eqn. (1). CPG: Central Pattern Generator.

For node	v_A	v_B	v_C	G_1	G_2	G_3
L1/C	$v_{5,R3/C}$	$v_{5,L2/C}$	$v_{5,R2/C}$	$-S_H/2$	$-S_H/2$	S_M+S_L
R2/C	$v_{5,L2/C}$	$v_{5,R1/C}$	$v_{5,L3/C}$	$-S_H/2$	$(S_M-S_H)/2$	$S_M/2+S_L$
L3/C	$v_{5,L2/C}$	$v_{5,R1/C}$	$v_{5,R3/C}$	S_M	S_L-S_H	0
R1/C	$v_{5,L2/C}$	$v_{5,R2/C}$	$v_{5,L3/C}$	S_M+S_L	$-S_H/2$	$-S_H/2$
L2/C	$v_{5,L1/C}$	$v_{5,R3/C}$	$v_{5,R2/C}$	$(S_M-S_H)/2$	$S_M/2+S_L$	$-S_H/2$
R3/C	$v_{5,L3/C}$	$v_{5,R2/C}$	$v_{5,L1/C}$	0	S_M	S_L-S_H

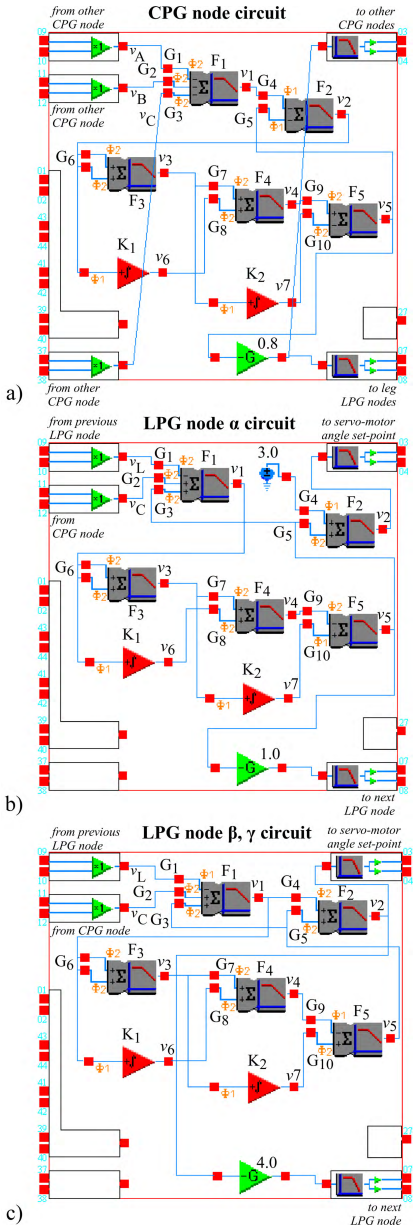

FIGURE 3. Non-linear oscillator structures. a) Oscillator circuit instanced at each CPG node (Eqn. (2)). b) First circuit variant, instanced at the LPG α nodes (Eqn. (4)). c) Second circuit variant, instanced at the LPG β and γ nodes (Eqn. (5)). See text for detailed descriptions.

where for better readability we have omitted the subscript referencing the CPG node label, i.e., $v_1 = v_{1,L1/C}$, $v_2 = v_{2,L1/C}$, etc. for node L1/C associated to leg L1, and so on. We note that the only non-linearity appearing in Eqn. (2) is the function $\Gamma(x, y)$, which represents saturation due to finite voltage swing according to

$$\Gamma(x, y) = \mathrm{R}(x)\,\mathrm{H}(V_s - y) - \mathrm{R}(-x)\,\mathrm{H}(V_s + y) \qquad (3)$$

where $\mathrm{H}(x) = 1$ for $x > 0$, 0 for $x \leq 0$ and $\mathrm{R}(x) = x\mathrm{H}(x)$.

Following empirical considerations, to realize self-sustained oscillation in each CPG node at a frequencies suitable for driving the physical robot in real-time, the filter frequencies are set to $F_1 = 15$ Hz, $F_2 = F_3 = F_4 = F_5 = 0.5$ Hz, the integration constants are set to $K_1 = 5.5 \times 10^{-6}$ μs^{-1} and $K_2 = 1.3 \times 10^{-6}$ μs^{-1}, the gains are set to $G_5 = -0.5$, $G_6 = 1.2$, $G_7 = 0.8$, $G_8 = 0.6$, $G_9 = 1.5$, $G_{10} = -0.4$, and with the intended target FPAA devices, the maximum voltage at any node is $|V_s| = 4$ V. Due to manufacturing tolerances, all parameters are subject to a random variation on the order of 0.1%-1% between nodes. Compared to the initial work wherein this circuit was introduced [26], here the parameter values and the coupling scheme are different, yielding oscillation at considerably lower frequencies and stable periodic orbits over a wide range of settings.

Given the presence of such large number of parameters and unavailability of a formal synthesis method, we proceeded as follows, starting from the circuit in [26]: 1) maintaining the original ring connectivity, the filter frequencies and integration constants were gradually scaled, in small steps, to bring oscillation from the low-kHz down to the low-Hz spectral region, 2) at each step, the gains were manually adjusted to maintain an approximately constant signal amplitude at each internal node, 3) after reaching the target frequency range, the connectivity was changed to that in Fig. 1 and the parameters were further tuned, one by one, to obtain the desired synchronization behavior in the CPG and LPG structures. Steps 1) and 2) were completed in simulations, since access to all internal nodes was necessary, whereas step 3) was completed deploying the oscillators to the physical circuit board, since consideration of the realistic behavior was necessary. The process was labor-intensive and relied on trial-and-error largely driven by intuitive appreciation of circuit and network behavior, representing a known issue associated to controller of this kind: at present there is still very limited knowledge about how to induce and manage desired emergent phenomena [5]–[8].

The only tunable parameters in the CPG nodes are the input gains G_1, G_2 and G_3, which are set according to Table 2,

and the internal gain $G_4 = -P_2$, where $P_2 \in [-1, 1]$ is the *activation parameter*, which provides control over whether to enable the CPG by setting $P_2 \approx 1$, disable it by setting $P_2 \approx 0$ or generate an approximately backwards gait pattern by setting $P_2 \approx -1$.

Since they are based on switched-capacitor circuits, FPAAs, albeit analog, are discrete-time devices, therefore in numerical simulations Eqn. (2) was accordingly discretized according to Euler's method, setting $\Delta\tau = 6.25$ ms as the fixed step size, corresponding to a switching rate of $f_c = 160$ Hz.

Two additional remarks on node dynamics are required. First, while minimizing the number of state variables is always desirable, given a predetermined oscillator circuit such as the present one the number of equations is inherently set by the circuit topology. In this case, the internal signals are clearly partially correlated, making the "effective" number of variables lower than the number of physical variables. Attempts to simplify the numerical model of the circuit are beyond the scope of this work, and from an implementation perspective we note that by design one circuit instance fits exactly into a single FPAA. Second, as discussed in [26] and in Sec. III, not all saturation nonlinearities present in Eqn. (2) are indispensable to support the generation of periodic orbits and stable gait patterns, those at the integrator outputs clearly prevailing over all others. Nevertheless, given that in the physical device saturation can occur for any variable, here we retained the $\Gamma(x, y)$ function in all equations.

3) LOCAL PATTERN GENERATORS (LPGs)

The architecture of the LPGs is inspired by the observation that in nature some situations and types of neurological damage (e.g., focal lesions involving motor circuits, blockade of certain receptor types) can produce uncoordinated leg movement, demonstrating the action of "local" circuits which can generate sustained activity even when deprived of the afferences from the CPG, and at the same time is driven by the aim of allowing flexible implementation of the available gaits through more than one power stroke delivery scheme, or "posture" [1], [2]. As shown in Fig. 1 and previously introduced, each LPG comprises three nodes, denoted with α, β and γ, whose outputs provide the position set-points for the servo-motors actuating the corresponding coxa-body, tibia-femur and femur-coxa joints of the associated leg.

The strength of coupling between each CPG node and the associated downstream LPG nodes is set by the *coupling strength parameter* $P_3 \in [0, 1]$; as demonstrated below, this parameter influences the level of synchronization between the outputs of the CPG and the corresponding downstream LPGs. When $P_3 \approx 1$, the temporal variance in the signals generated by each LPG is almost entirely determined by the CPG input (extrinsic activity, supported by the connections represented as yellow arrows in Fig. 1), whereas when $P_3 \approx 0$, the LPG nodes oscillate spontaneously and asynchronously with respect to CPG activity, therefore without stable phase relationships between the legs, leading to a "thrashing-like" uncoordinated movement (intrinsic activity, supported by the connections represented as purple arrows in Fig. 1).

The LPGs are also controlled via the *posture parameter* $P_4 \in [0, 1]$, which enables transitioning between the ant-like and cockroach-like postures: for $P_4 \approx 0$ (ant-like posture), the power stroke is delivered by the coxa-body joint of all legs, whereas for $P_4 \approx 1$ (cockroach-like posture), the front and hind legs deliver the power stroke primarily using the tibia-femur joint, in opposite directions. Finally, the *steering parameter* $P_5 \in [-1, 1]$ enables steering the trajectory of the robot sideways by reducing the power stroke amplitude on either side.

The parameters P_3, P_4 and P_5, together with a set of constants specified below, influence the dynamics of the LPG nodes through the gains $G_1, G_2, \ldots, G_5$ in the LPG circuits, shown in Figs. 3b and c. These circuits present minor structural differences with respect to the CPG oscillators; in particular, the LPGα nodes, controlling the coxa-body joints, have the capability of adding a large offset V_r to the output, which is necessary to make the front and rear legs "spread out" with respect to the body, whereas the LPGβ and LPGγ nodes, controlling the other two joints, have the capability of mixing the output of the ring v_5 directly with the summation of the external inputs v_1, which is referred to as "mixed output" and necessary to realize all desired phase relationships between the joints.

For the LPGα oscillators (Fig. 3b), the resulting system of ordinary differential equations can be written as follows:

$$\begin{cases} \dfrac{dv_1}{dt} = \Gamma\Big(2\pi F_1(G_1 v_L + G_2 v_C + G_3 v_5 - v_1), v_1\Big) \\ \dfrac{dv_2}{dt} = \Gamma\Big(2\pi F_2(G_4 V_r + G_5 v_5 - v_2), v_2\Big) \\ \dfrac{dv_3}{dt} = \Gamma\Big(2\pi F_3(G_6 v_1 - v_3), v_3\Big) \\ \dfrac{dv_4}{dt} = \Gamma\Big(2\pi F_4(G_7 v_3 + G_8 v_6 - v_4), v_4\Big) \\ \dfrac{dv_5}{dt} = \Gamma\Big(2\pi F_5(G_9 v_4 + G_{10} v_7 - v_5), v_5\Big) \\ \dfrac{dv_6}{dt} = \Gamma\Big(K_1 v_1, v_6\Big) \\ \dfrac{dv_7}{dt} = \Gamma\Big(K_2 v_3, v_7\Big) \end{cases} \tag{4}$$

where $F_2 = 15$ Hz, $G_9 = -1.5$, $G_{10} = 0.4$, $V_r = 3$ V and all other parameters are set as for the CPG nodes.

For the LPGβ and LPGγ oscillators (Fig. 3c), the resulting system of ordinary differential equations can be written

as follows:

$$\begin{cases} \frac{dv_1}{dt} = \Gamma\Big(2\pi F_1(G_1 v_L + G_2 v_C + G_3 v_5 - v_1), v_1\Big) \\ \frac{dv_2}{dt} = \Gamma\Big(2\pi F_2(G_4 v_1 + G_5 v_5 - v_2), v_2\Big) \\ \frac{dv_3}{dt} = \Gamma\Big(2\pi F_3(G_6 v_1 - v_3), v_3\Big) \\ \frac{dv_4}{dt} = \Gamma\Big(2\pi F_4(G_7 v_3 + G_8 v_6 - v_4), v_4\Big) \\ \frac{dv_5}{dt} = \Gamma\Big(2\pi F_5(G_9 v_4 + G_{10} v_7 - v_5), v_5\Big) \\ \frac{dv_6}{dt} = \Gamma\Big(K_1 v_1, v_6\Big) \\ \frac{dv_7}{dt} = \Gamma\Big(K_2 v_3, v_7\Big) \end{cases} \quad (5)$$

without further changes to the parameters.

In all LPG nodes, the gains G_1, G_2 and G_3 are determined by parameters P_3 and P_4 according to the B parameters defined by the expressions in Table 4: G_2 controls the coupling of the LPGs to the CPG, whereas G_1 and G_3 respectively control the interdependence between the nodes of each LPG and the internal loop gain within each node; variable v_L corresponds to the output voltage of the previous node in the LPG ring (i.e., voltage $-v_5$ for $\alpha \rightarrow \beta$ coupling, $-4v_2$ for $\beta \rightarrow \gamma$ and $\gamma \rightarrow \alpha$ coupling), and variable v_C corresponds to the v_5 voltage of the CPG node associated to the LPG (see Fig. 1).

The expressions in Table 4 represent the linear superposition of three distinct canonical configurations, controlled by different B parameter subsets. To aid the understanding of these parameters, individual descriptions are provided in Table 5. First, the phase relationships required for walking in the ant-like posture ($P_3 = 1$, $P_4 = 0$) are implemented as follows: 1) the LPG α and β nodes of all legs receive the afferent signal from the associated CPG node, 2) the LPG γ nodes of all legs instead receive the output of the corresponding β node, and 3) the LPG α and γ nodes of all legs have non-zero internal loop gain. Second, the phase relationships required for walking in the cockroach-like posture ($P_3 = P_4 = 1$) are implemented as follows: 1) the LPG α and β nodes of all legs and the γ nodes of the front and hind legs (opposite phase) receive the afferent signal from the associated CPG node, 2) the LPG γ nodes of the middle legs instead receive the output of the corresponding β node, and 3) the LPG α and γ nodes have non-zero internal loop gain for the middle legs, whereas the LPG β nodes have non-zero internal loop gain for the front and hind legs. Third, uncoordinated movement ($P_3 = 0$) is implemented as follows: 1) there is no input from the CPG, 2) the LPG nodes are coupled forming the following loop $\alpha \rightarrow \beta \rightarrow \gamma \rightarrow \alpha$, and 3) the LPG α nodes of all legs have non-zero internal loop gain.

Similarly, the gains G_4 and G_5 are determined by parameters P_3, P_4 and P_5 according to the C parameters defined by the expressions in Table 6; together, G_4 and G_5 influence how the servo-motor position signals, corresponding to voltage v_2, are obtained from the internal voltages v_1 and v_5. To simplify the notation in Tables 4 and 6, we have set $P'_3 = 1 - P_3$, $P'_4 = 1 - P_4$, $P'_5 = 1 - R(-P_5)$ and $P''_5 = 1 - R(P_5)$.

The expressions in Table 6 also represent the linear superposition of three distinct canonical configurations, controlled by different C parameter subsets. To aid the understanding of these parameters, individual descriptions are provided in Table 7. First, the LPG→servo-motor connectivity required for walking in the ant-like posture ($P_3 = 1$, $P_4 = 0$) is implemented as follows: 1) the α joint servo-motors of all legs have no offset (coxa-body angle zero-point is such that the legs do not "spread out"), 2) the α joint servo-motors of all legs are driven by the corresponding LPG direct outputs, 3) the β and γ joint servo-motors of all legs are driven by the corresponding LPG mixed outputs. Second, the LPG→servo-motor connectivity required for walking in the cockroach-like posture ($P_3 = P_4 = 1$) is implemented as follows: 1) the α joint servo-motors of the front and hind legs are held in fixed positions with negative and positive offsets respectively (these legs "spread out"), 2) the α joint servo-motors of the middle legs are driven by the corresponding LPG direct outputs, 3) the β joint servo-motors of the front and hind legs are driven by the corresponding LPG direct outputs, those of the middle legs are driven by the corresponding LPG mixed outputs, 4) the γ joint servo-motors of all legs are driven by the corresponding LPG mixed outputs. Third, the LPG→servo-motor connectivity required for uncoordinated movement ($P_3 = 0$) is implemented in the same manner as walking in the ant-like posture, but with different parameter settings. In addition, steering (P_5) is implemented exclusively by reducing power stroke width, on the α or β joints for ant- and cockroach-like walking respectively.

4) PARAMETER DETERMINATION

To drive the experimental robot described in the next section, the constants in Table 4 and 6 are empirically set as follows: $B_1 = 1.2$, $B_2 = 1.5$, $B_3 = B_5 = -B_9 = 0.8$, $B_4 = -2$, $B_6 = -2.2$, $B_7 = 3$, $B_8 = 2$, $C_1 = -0.28$, $C_2 = -C_3 = C_{12} = -C_{13} = C_{20} = -C_{21} = 0.04$, $C_4 = C_5 = -C_6 = C_7 = C_{14} = -C_{15} = C_{22} = C_{23} = -C_{24} = C_{25} = 0.1$, $C_8 = C_{16} = C_{26} = 0.36$, $C_9 = C_{17} = C_{19} = C_{27} = 0.3$ and $C_{10} = -C_{11} = -C_{18} = C_{28} = -C_{29} = 0.2$.

The procedures for determining these parameters are described in the Appendix. It should be noted that these settings plausibly do not represent neither a unique nor an optimal solution. They were not subject to any optimization or robustness assessment; they simply reflect a configuration of the controller which is viable for the specific robot under consideration. In future deployments of the controller, these parameter settings may be tuned using techniques such as genetic algorithms, as described in [18], and even the parameter formulations can likely be improved. While targeting different mechanics could require extensive re-determination of the C parameters, the B parameter settings plausibly represent a starting point of good general validity.

B. DYNAMICS

1) INITIAL SIMULATIONS AND PHYSICAL IMPLEMENTATION

To have access to all internal voltages $v_1, \ldots, v_7$ of each node, the CPG subnetwork was initially simulated according to Eqns. (1)-(3) using a fixed-step solver and the parameter settings prescribed above. Generation of the expected gait patterns at low, medium and high settings of P_1 was observed. However the wave gait was initially obscured by onset of global synchronization [24], which was manifest as in-phase movement of all legs (data not shown). This could be avoided by having random $v_i(0) \in [-V_s, V_s]$ and adding a Gaussian random variation in the CPG parameters having a standard deviation of 0.5%, a situation which recalls observations from the initial study on this oscillator, wherein parametric mismatches were fundamental for the emergence of structured synchronization patterns instead of global synchronization [26]. Consideration of the individual voltage time-series, exemplified in Figs. 4a and b, indicated that saturation to $\pm V_s$ appeared primarily at the integrator outputs v_6 and v_7 (and, for low settings of P_1, also at v_5), which is in agreement with the observations reported in [26], despite the widely different parameter settings. Indeed, the presence of nonlinearity primarily or solely in the form of saturation is a recurring feature across many of the known FPAA-based nonlinear oscillators [33].

The entire network shown in Fig. 1 was thereafter physically implemented on the LYAPUNOV-1 circuit board, which effectively constitutes a reconfigurable analog machine in the form of a plug-in card for a standard desktop computer; it provides 32 FPAAs alongside supporting infrastructure for real-time data acquisition and dynamic reconfiguration of all analog circuit parameters. The design is publicly available and described in detail in [26] and [35]; here, the FPAA interconnections on the circuit board were manually rewired as pictured in Fig. 5a, and detailed in the online materials [36]. Compared to numerical simulations, deployment on physical hardware knowingly results in richer dynamics, for example due to parametric mismatches, non-ideal behavior of circuit elements and noise; in particular, physically $\Gamma(x, y)$ does not correspond to an ideal step function due to more complex circuit behavior as saturation is approached [26], [33].

Since FPAAs are switched-capacitor circuits, and hence have discrete-time dynamics, it is possible to effectively "rescale" the temporal dynamics simply by changing the clock frequency $f_c = 1/\Delta\tau$ within the range allowed by the hardware, representing a notable advantage in comparison to circuits built with discrete components [4], [20], [33]; in this work, all experiments not involving real-time control of the physical robot were performed with a time-step reduced by a factor of 5 to limit the acquisition time.

2) GAIT PATTERN GENERATION

To test gait pattern generation on the physical oscillator network, the parameter P_1 was first continuously swept in a cycle between 0 and 1, dynamically changing in small steps the gains G_1, G_2 and G_3 according to Table 2. As shown in Fig. 4c, the CPG responded gradually, generating initially the wave gait for $P_1 < 0.25$, then the tetrapod (metachronal) gait for $0.25 < P_1 < 0.45$, then a "paradoxical" intermediate gait featuring inversion of the phase relationships between legs L3-R1 and R3-L1 for $0.45 < P_1 < 0.65$, then disordered activity for $P_1 \approx 0.65$ and finally the tripod gait for $P_1 > 0.75$; a hysteresis effect was also observed, as described in detail below. Corresponding gait patterns observed when starting and operating the CPG at constant P_1 settings are shown in Figs. 6a-g and were largely similar, albeit with some deviation in the unstable region around $P_1 \approx 0.65$. These results confirm that the CPG is capable of expressing a generalized gait as a function of P_1, featuring not only the hardwired canonical gaits, but also additional emergent intermediate gaits which, as demonstrated in the following section, were kinematically viable. This result is particularly noteworthy, as it confirms the ability of the controller to generate behaviors beyond the hardwired ones. The raw time-series recorded at all network nodes are publicly available [36].

The ability of the CPG to respond to abrupt parameter changes was subsequently tested by dynamically altering P_1 and P_2 in large steps. The results, exemplified in Figs. 4d and e, demonstrated that the CPG was able to rapidly switch between gaits without instability, as well as to inhibit and resume oscillation reliably. However, while the gait changes shown in Fig. 4d were near-immediate, the build-up of oscillations starting from an "isoelectric" condition was gradual, requiring a time-interval equivalent to several cycles. As better illustrated in Figs. 7a and 8a respectively for $P_1 = 0.8$ and $P_1 = 0.2$, the tripod gait emerged slowly through the build-up of initially disordered oscillations which eventually developed the desired phase relationships, whereas the wave gait emerged more rapidly, through symmetry breaking caused by one node which, after a certain delay, generated a large fluctuation and triggered the wave. As shown in Fig. 4e, sudden transition to an approximately reverse gait induced by setting $P_2 = -1$ caused a perturbation persisting for a time interval similar to that required for initial oscillation build-up. Even though these phenomena are in themselves interesting, they could be viewed as a shortcoming when rapid controllability is the purpose; in such cases, the role of feedback through sensory signals from peripheral receptors becomes important for speeding up convergence towards the desired steady-state solution. Injecting a suitable transient in the oscillator parameters, e.g. with $P_2 > 1$, could also represent a viable approach to implement faster start-up.

3) TRANSITIONS AND SYNCHRONIZATION

To gain further insight into the transitions between the gaits, the continuous phase of each leg $\varphi_i(t)$ was extracted by calculating, for each of the six CPG outputs $i \in$ L1/C, R2/C, ..., R3/C, the corresponding analytic signal

as follows

$$v_{5,i}(t) + \mathrm{i}\hat{v}_{5,i}(t) = A_i(t)\mathrm{e}^{\mathrm{i}\varphi_i(t)} \tag{6}$$

where $\hat{v}_{5,i}$ is the Hilbert transform of $v_{5,i}(t)$

$$\hat{v}_{5,i}(t) = \frac{1}{\pi}\mathrm{p.v.}\left[\int_{-\infty}^{\infty}\frac{v_{5,i}(\tau)}{t-\tau}\mathrm{d}\tau\right] \tag{7}$$

and where p.v. denotes the Cauchy principal value of the integral [37].

The characterize each gait, predicated on Wilson's rules [1], [2], the following summary parameter was introduced

$$\zeta = \frac{\Delta\varphi_1 + \Delta\varphi_2 - \Delta\varphi_3 + \Delta\varphi_4 + \Delta\varphi_5 - \Delta\varphi_6}{\sum\Delta\varphi} \tag{8}$$

where

$$\begin{cases} \Delta\varphi_1 = |\langle\varphi_{\mathrm{L1/C}}(t) - \varphi_{\mathrm{R2/C}}(t)\rangle_{\Delta t}| \\ \Delta\varphi_2 = |\langle\varphi_{\mathrm{R2/C}}(t) - \varphi_{\mathrm{L3/C}}(t)\rangle_{\Delta t}| \\ \Delta\varphi_3 = |\langle\varphi_{\mathrm{L3/C}}(t) - \varphi_{\mathrm{R1/C}}(t)\rangle_{\Delta t}| \\ \Delta\varphi_4 = |\langle\varphi_{\mathrm{R1/C}}(t) - \varphi_{\mathrm{L2/C}}(t)\rangle_{\Delta t}| \\ \Delta\varphi_5 = |\langle\varphi_{\mathrm{L2/C}}(t) - \varphi_{\mathrm{R3/C}}(t)\rangle_{\Delta t}| \\ \Delta\varphi_6 = |\langle\varphi_{\mathrm{R3/C}}(t) - \varphi_{\mathrm{L1/C}}(t)\rangle_{\Delta t}| \end{cases} \tag{9}$$

and where $\langle\rangle$ denotes the temporal average over a sufficiently long observation time, i.e. $\Delta t \gg \Delta\tau$. As shown in Fig. 4f, $\zeta > 0$ for the wave, tetrapod (metachronal) and intermediate gaits, peaking at $\zeta \approx 1$ for $P_1 \approx 0.4$, whereas $\zeta < 0$ for the tripod gait. Consideration of this parameter revealed clear hysteresis in the transition between the slower gaits and the tripod gait, which occurred in the region of $0.6 < P_1 < 0.7$: depending on the sweep direction, the summary parameter ζ flipped sign at different points, namely $P_1 \approx 0.63$ and $P_1 \approx 0.67$, and the disturbance accompanying the transition manifested with different phase relationships between the legs. In contrast with that between the wave and the tetrapod (metachronal) gait, this transition was therefore not smooth, plausibly because it involved "competition" between links having positive (S_{L}, S_{M}) and negative (S_{H}) weights, as per Table 2. In addition to hysteresis, metastability, that is presence of states with a finite life-time, was observed, as exemplified for $P_1 \approx 0.66$ in Fig. 4h. The transition was therefore unequivocally a first-order one. These phenomena, which were not explicitly designed for but spontaneously emerged from the connectivity and dynamics, are particularly striking as they mirror experimental observations on the transition between the same gaits in living insects and mathematical models predicated on completely different formulations (for example, see [38]).

Similarly, as shown in Fig. 4g, the emergent period of the gaits τ, defined on the basis on the first peak of the autocorrelation function, was lowest for the tripod gait, which in nature is generally associated with fast walking [2]; as expected, τ diverged in the region of the hysteretic transition.

We subsequently considered the level of synchronization, expressed in terms of phase-locking according to

$$r_{i,j} = |\langle\mathrm{e}^{\mathrm{i}[\varphi_i(t)-\varphi_j(t)]}\rangle| \tag{10}$$

where $r_{i,j} \in [0, 1]$ (the extreme values representing, respectively, complete asynchrony or presence of a perfect phase relationship, regardless of the relative phase angle and of cycle amplitude, between two oscillators i and j [39]).

First, this parameter was calculated and averaged between all CPG node pairs (voltages v_5 in Fig. 3a), according to

$$\begin{aligned}\langle r_{\mathrm{C}}\rangle = (&r_{\mathrm{L1/C,R2/C}} + r_{\mathrm{L1/C,L3/C}} + r_{\mathrm{L1/C,R1/C}} \\ &+ r_{\mathrm{L1/C,L2/C}} + r_{\mathrm{L1/C,R3/C}} + r_{\mathrm{R2/C,L3/C}} + r_{\mathrm{R2/C,R1/C}} \\ &+ r_{\mathrm{R2/C,L2/C}} + r_{\mathrm{R2/C,R3/C}} + r_{\mathrm{L3/C,R1/C}} + r_{\mathrm{L3/C,L2/C}} \\ &+ r_{\mathrm{L3/C,R3/C}} + r_{\mathrm{R1/C,L2/C}} + r_{\mathrm{R1/C,R3/C}} + r_{\mathrm{L2/C,R3/C}})/15\end{aligned} \tag{11}$$

which indicated that oscillations remained strongly coherent among the CPG nodes, i.e. $\langle r_{\mathrm{C}}\rangle \approx 1$, for all settings of P_1 except in proximity of the hysteretic transition, where, as discussed above, activity became disordered and the period τ accordingly diverged (data not shown).

Second, phase variables for the LPG nodes were introduced in a way similar to Eqn. (6), considering the voltage v_2 for nodes L1/α, L2/α, ..., R3/α (Fig. 3b) in order to define $\varphi_{\mathrm{L1}/\alpha}, \ldots, \varphi_{\mathrm{R3}/\alpha}$, and so on for the β and γ nodes (Fig. 3c). The phase-locking index as in Eqn. (10) was thereafter calculated between each CPG node and the three associated downstream LPG α, β and γ nodes, and averaged across all six legs according to

$$\begin{aligned}\langle r_{\mathrm{C}\to\mathrm{L}}\rangle = (&r_{\mathrm{L1/C,L1}/\alpha} + r_{\mathrm{L1/C,L1}/\beta} + r_{\mathrm{L1/C,L1}/\gamma} \\ &+ r_{\mathrm{R2/C,R2}/\alpha} + r_{\mathrm{R2/C,R2}/\beta} + r_{\mathrm{R2/C,R2}/\gamma} \\ &+ r_{\mathrm{L3/C,L3}/\alpha} + r_{\mathrm{L3/C,L3}/\beta} + r_{\mathrm{L3/C,L3}/\gamma} \\ &+ r_{\mathrm{R1/C,R1}/\alpha} + r_{\mathrm{R1/C,R1}/\beta} + r_{\mathrm{R1/C,R1}/\gamma} \\ &+ r_{\mathrm{L2/C,L2}/\alpha} + r_{\mathrm{L2/C,L2}/\beta} + r_{\mathrm{L2/C,L2}/\gamma} \\ &+ r_{\mathrm{R3/C,R3}/\alpha} + r_{\mathrm{R3/C,R3}/\beta} + r_{\mathrm{R3/C,R3}/\gamma})/18\end{aligned} \tag{12}$$

As shown in Fig. 4i, this parameter responded to P_1 in a manner similar to $\langle r_{\mathrm{C}}\rangle$, largely irrespective of the posture setting (i.e., $P_4 = 0$ vs. $P_4 = 1$). As shown in Fig. 4j, the same gradually increased with the coupling strength P_3, which set the unidirectional energy transfer rate maintaining synchronization between the CPG and the LPGs; for $P_3 > 0.3$, complete synchronization was consistently observed, with $\langle r_{\mathrm{C}\to\mathrm{L}}\rangle \approx 1$, whereas at lower P_3 settings two different critical coupling strengths could be observed, corresponding to $P_3 \approx 0.1$ for the wave gait and $P_3 \approx 0.3$ for the tripod gait [24].

Altogether, these results confirm i) the synchronizability of the hierarchical oscillator network across all gaits, and ii) the ability to gradually transition the LPGs between a configuration in which they generate "intrinsic" activity unsynchronized to the CPG (low P_3) and one in which they closely track the "extrinsic" input from the CPG (high P_3).

The raw time-series recorded for all network nodes are publicly available [36].

III. EXPERIMENTAL DEPLOYMENT

A. ROBOT DESIGN AND DATA ACQUISITION

To demonstrate the viability of the proposed controller experimentally, the same was deployed to perform real-time open-loop control of an ant-like hexapod robot, named 非線形蟻-1 (*hisenkei ari*-1), derived from the *A-Pod* design by Kåre Halvorsen (a.k.a. ''Zenta''; marketed by Lynxmotion Inc., Swanton VT). The robot, shown in Fig. 5b, was equipped with six identical legs, each providing three degrees of freedom corresponding, as discussed above, to the coxa-body (α), tibia-femur (β) and femur-coxa (γ) joints. The robot included additional joints for the mandibles and tail, which were not used in the present experiment and were set to constant angles. Each axis was actuated by an HS-645MG servo-motor (Hitec RCD Inc., Chungcheongbuk-do, South Korea), providing a maximum stall torque of 9.6 kg · cm. The robot was 65 cm long and 45 cm wide, and weighted 3.25 kg; the tibia and femur were respectively 14 cm and 10.5 cm long. The center-of-mass was ≈ 2 cm forward of the middle legs, and the body raised 9 cm above the base plate. The robot was powered by a 5000 mAh, 6.0 V nickel-metal hydride battery pack.

The LYAPUNOV-1 circuit board (Fig. 5a) was installed in a desktop computer running Linux, and the experiment was programmed using MATLAB and C code. A first thread managed FPAA array configuration and real-time data acquisition, and forwarded via TCP/IP the FPAA output measurements (digitized at 12-bit, 160 Hz) to a second thread, which performed down-sampling from 160 Hz to 16 Hz, linear mapping to the individual servo-motor angles (calibration), enforced joint angle limits and streamed the signals to the robot via a dedicated radio link. A third thread gathered telemetry and video data. The robot was locally controlled by a network of five ATmega328 micro-controllers (Microchip Technology Inc., San Jose CA), programmed in the Arduino environment (Arduino S.r.l., Ivrea TO, Italy), which implemented motor control, sensor interfacing and radio communication functions. The robot was interfaced to the computer by means of an isochronous frame-based protocol updating at 16 frames/second and deployed over separate up- and down-link channels (APC220; AppCon Technologies, Shenzhen, China). All source code is publicly available [36].

Pitch and roll data were gathered from an inertial motion unit (IMU) based on direction cosine matrix (DCM) formation (9 DoF Razor IMU; SparkFun Inc., Niwot CO) [40]. To perform visual odometry, stereoscopic images were acquired from a camera (BlackBird 2; FPV3DCAM, Moscow, Russia) mounted above the mandibles, having focal length 2.5 mm, stereo base 42 mm and resolution 680 × 512 per eye, which was synchronized with the acquisition of telemetry data from all other sensors. The robot was operated over a smooth floor in an indoor environment where additional landmarks had been installed; as discussed below, this represents an important limitation of this initial study, in that the open-loop configuration did not provide any adaptiveness which would allow locomotion over irregular terrain. The elevation of the body over the ground was not derived from the video data, and instead it was directly measured with higher precision by means of a time-of-flight laser sensor installed under the bottom plate (VL53L0X; STMicroelectronics S.p.A., Agrate Brianza MI, Italy).

The video frames were de-multiplexed, de-interlaced, converted to gray-scale and undistorted, after which feature identification and matching was performed by means of the speeded-up robust features (SURF) technique [41]. Camera rotation and translation were thereafter estimated using the maximum likelihood estimation sample consensus (MLESAC) approach, derived from the RANSAC estimator [42]. Following initial evaluation, it was decided to perform monocular odometry separately for the two cameras, combining the respective processed data for each frame, iteratively choosing the time-span for motion estimation, and applying median filtering to the six resulting series of Euler angles and displacements. To improve accuracy, distance calibration was performed separately for each experimental run, taking as reference a forward-facing ultrasonic sensor mounted under the mandibles (MB1242; MaxBotix Inc., Brainerd MN). Because accuracy validation was not performed, the odometry data should nevertheless be considered as merely illustrative.

To gain further insight into the stability of the gaits, each femur was instrumented with a strain gage (MMF003247; Micro-Measurements Inc., Wendell NC) sensitive to longitudinal strain, and connected to an operational amplifier installed proximally. The resulting time-series $\varepsilon_i(t)$ provided an indication of the level of strain in the plastic structure of the legs, induced by both acceleration and contact with the terrain. As specified in the next subsection, the focus was on the temporal regularity, hence no calibration was performed and the values were treated as arbitrary units.

B. ANALYSES AND RESULTS

Initial experiments were performed suspending the robot atop an elevated platform, which allowed optimal observation of the phase relationships between the legs; as documented in Fig. 6 and associated video materials [36], the actuators successfully reproduced the gait patterns generated for $P_1 \in [0.2, 0.8]$, $P_2 = P_3 = 1$, $P_4 = P_5 = 0$. Subsequently, the robot was exercised in 22 experimental runs on indoor environment, detailed in Table 3, which spanned the same range of P_1 separately in the ant-like and cockroach-like postures, i.e. $P_4 = 0$ and 1 respectively, and additionally covered the cases of steering, i.e. $P_5 = -1$, and uncoordinated movement, i.e. $P_3 = 0$ (see Table 1 for parameter definitions).

In the absence of external perturbation of the control parameters, if the controller is stable one expects the generation of a perfectly regular (i.e., periodic) gait pattern. An empirical approach to testing this hypothesis is by means of quantifying how much variance in the generated

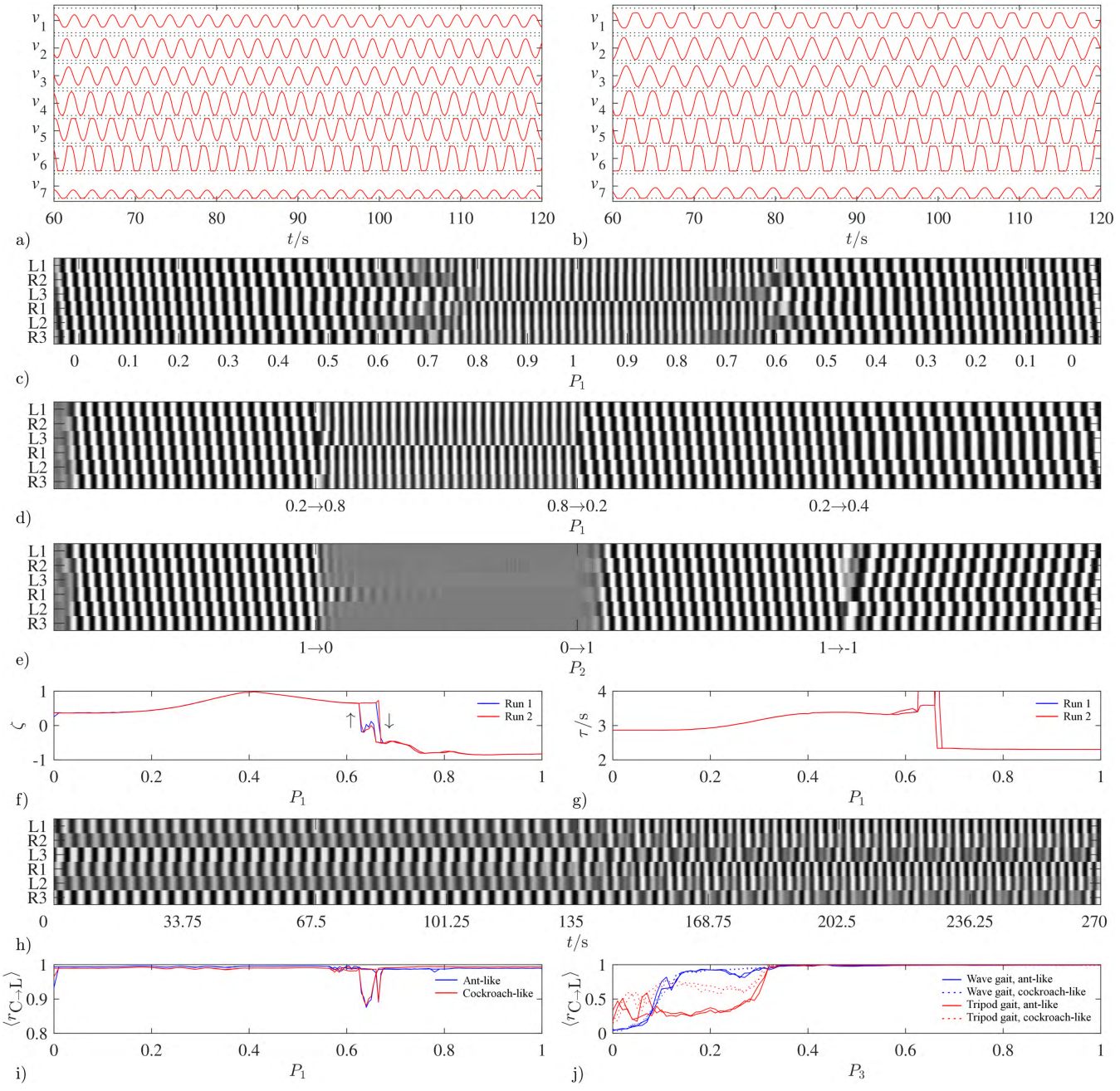

FIGURE 4. **Central pattern generator (CPG) dynamics. a) and b) Simulated time-series from all internal voltages of a representative CPG node, respectively for gait selection parameter settings $P_1 = 0.8$ and $P_1 = 0.2$. c) Gait diagram, representing experimental CPG output time-series, for a continuous cycle $P_1 = 0 \rightarrow 1 \rightarrow 0$ in 0.1 steps; black and white areas respectively denote the swing and stance phases; data length for each parameter setting step $\Delta t \approx 13$ s. d) and e) Gait diagrams, respectively for sharp transitions of the gait selection parameter $P_1 = 0.2 \rightarrow 0.8 \rightarrow 0.2 \rightarrow 0.4$ and of the activation parameter $P_2 = 1 \rightarrow 0 \rightarrow 1 \rightarrow -1$; data length for each parameter setting step $\Delta t \approx 60$ s. f) and g) Gait summary parameter ζ and period τ as a function of P_1; blue and red: distinct identical runs. A complete cycle $P_1 = 0 \rightarrow 1 \rightarrow 0$ is charted, and vertical arrows denote the direction of discontinuous transition for ζ. h) Gait diagram exemplifying spontaneous transition observed for $P_1 = 0.66$. i) Average phase synchronization between the CPG and corresponding LPG nodes $\langle r_{C \rightarrow L} \rangle$ as a function of P_1; blue and red: ant-like and cockroach-like postures, i.e. posture parameter $P_4 = 0$ and $P_4 = 1$, respectively. A complete cycle $P_1 = 0 \rightarrow 1 \rightarrow 0$ is charted. j) Same parameter $\langle r_{C \rightarrow L} \rangle$ as a function of the coupling strength parameter P_3; blue and red: wave and tripod gaits, i.e. $P_1 = 0.2$ and $P_1 = 0.8$, respectively, solid and dashed: ant-like and cockroach-like postures, i.e. $P_4 = 0$ and $P_4 = 1$, respectively. A complete cycle $P_3 = 0 \rightarrow 1 \rightarrow 0$ is charted. Unless otherwise specified $P_2 = P_3 = 1$. Corresponding data files available online [36].**

time-series $s_i(t)$ can be expressed as a partial Fourier series up to a given finite number of terms k. Such *periodicity ratio* may be written as follows

$$\eta = \langle \sigma^2[\hat{s}_i(t)] / \sigma^2[s_i(t)] \rangle_{i \in \mathrm{L1,R2,\ldots,R3}} \tag{13}$$

where $\sigma^2[s(t)]$ denotes the variance of $s(t)$ for $0 < t < t_{\max}$, and the corresponding partial Fourier series

$$\hat{s}(t) = \frac{a_0}{2} + \sum_{n=1}^{k} a_n \cos(nt) + \sum_{n=1}^{k} b_n \sin(nt) \tag{14}$$

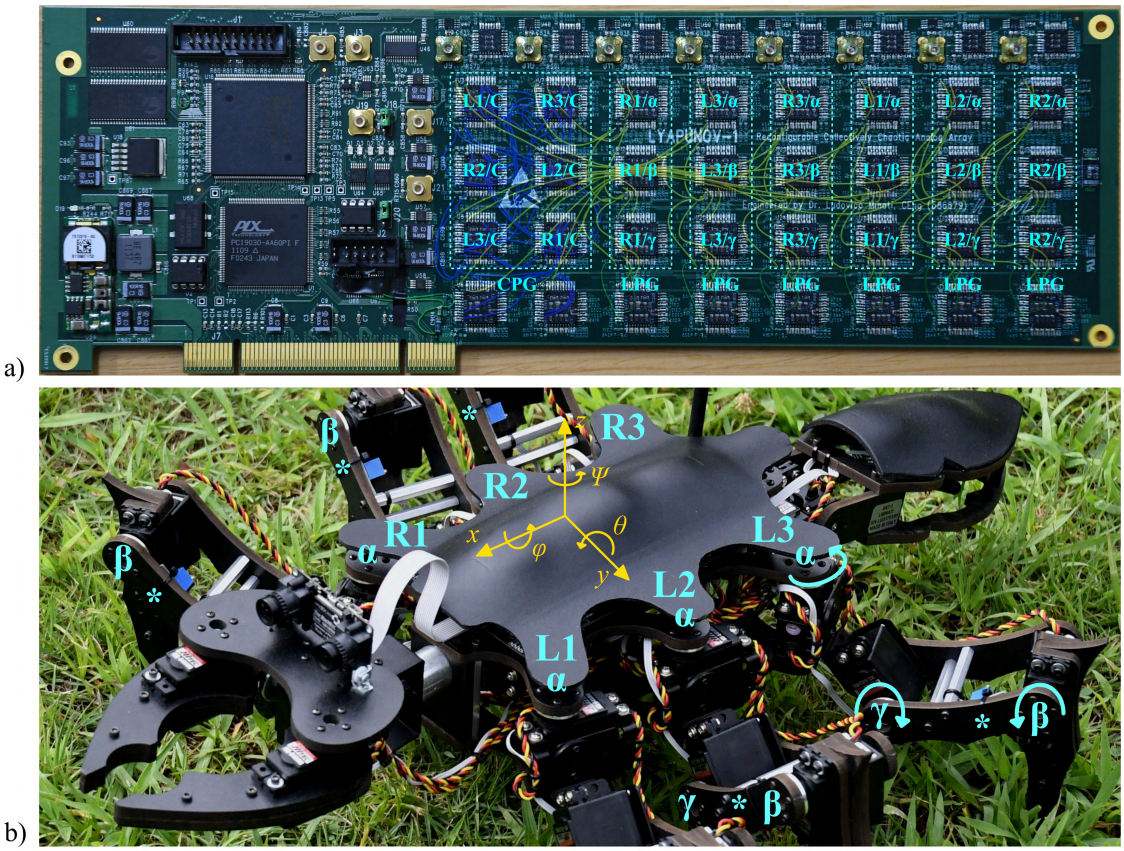

FIGURE 5. Experimental setup. a) Semi-transparent view of the LYAPUNOV-1 board, depicting the allocation of network nodes to FPAAs, and the re-wiring implementing the CPG and LPG links (blue, yellow). b) Hexapod robot, featuring independent coxa-body (α), femur-coxa (γ) and tibia-femur (β) joints for each leg. Locations of the strain gages for measuring the femur longitudinal strains ε_i are indicated by "*". CPG: Central Pattern Generator. FPAA: Field-Programmable Analog Array. LPG: Local Pattern Generator.

where, in the present case, we set $k = 8$ and a_n and b_n were estimated by robust non-linear least-squares optimization over multiple runs. The periodicity ratio η can be considered as an order parameter, since one expects $\eta \approx 0$ and 1, respectively, for stochastic and ordered dynamics. Away from the transition region and given sufficient time for initial transient stabilization, i.e. for large $t_{\max}$, for all CPG and LPG outputs we observed $\eta \approx 1$, even though slow oscillations extending beyond the gait period occasionally emerged at some LPG outputs, plausibly due to parametric mismatches (data not shown). This result confirmed that the outputs of the hierarchical controller have a high level of periodicity, i.e. gait generation is largely stable. It was however noted that oscillation start-up for $P_1 = 0.6$ occasionally fails, highlighting a form of instability in the transition region.

An "idealized" walking robot reacts immediately to the controller outputs and has no memory, thus when driven by perfectly regular signals, all of its physical variables change in an identical manner between each gait cycle and the next one. However, a physical robot such as the present one has a certain weight distribution, finite joint torques, elasticity and a number of non-idealities, meaning that it may not be able to reproduce faithfully the controller outputs, for example if the gait period τ is too short, which may lead to structural instability evident in the form of fluctuations between one gait cycle and the next. To investigate this aspect, the parameter η was calculated from the femur strain signals $\varepsilon_i(t)$ recorded in all gaits and postures. For this and the subsequent analyses, segments of undisturbed walking (i.e., excluding the initial transient, contact with obstacles etc.) were manually segmented from the experimental data and concatenated. As indicated in Table 3, the observed values were overall high, i.e. $\eta \approx 0.9$, suggesting that the robot could successfully reproduce the prescribed gait patterns, however some intermediate gaits and the tripod gait were relatively unstable in the cockroach-like posture (i.e., runs $n = 15 \ldots 18$). As expected, during uncoordinated movement (i.e., runs $n = 21, 22$) the leg strain signals were temporally disordered, i.e. $\eta \approx 0.5$.

Representative gait patterns, leg joint position signals, trajectories and video frame sequences for walking in the ant-like and cockroach-like postures are shown, respectively, in Figs. 7a-e and Figs. 8a-e. The leg trajectories in the space of the $[\alpha, \beta, \gamma]$ joint angles, visible in Fig. 7c and Fig. 8c,

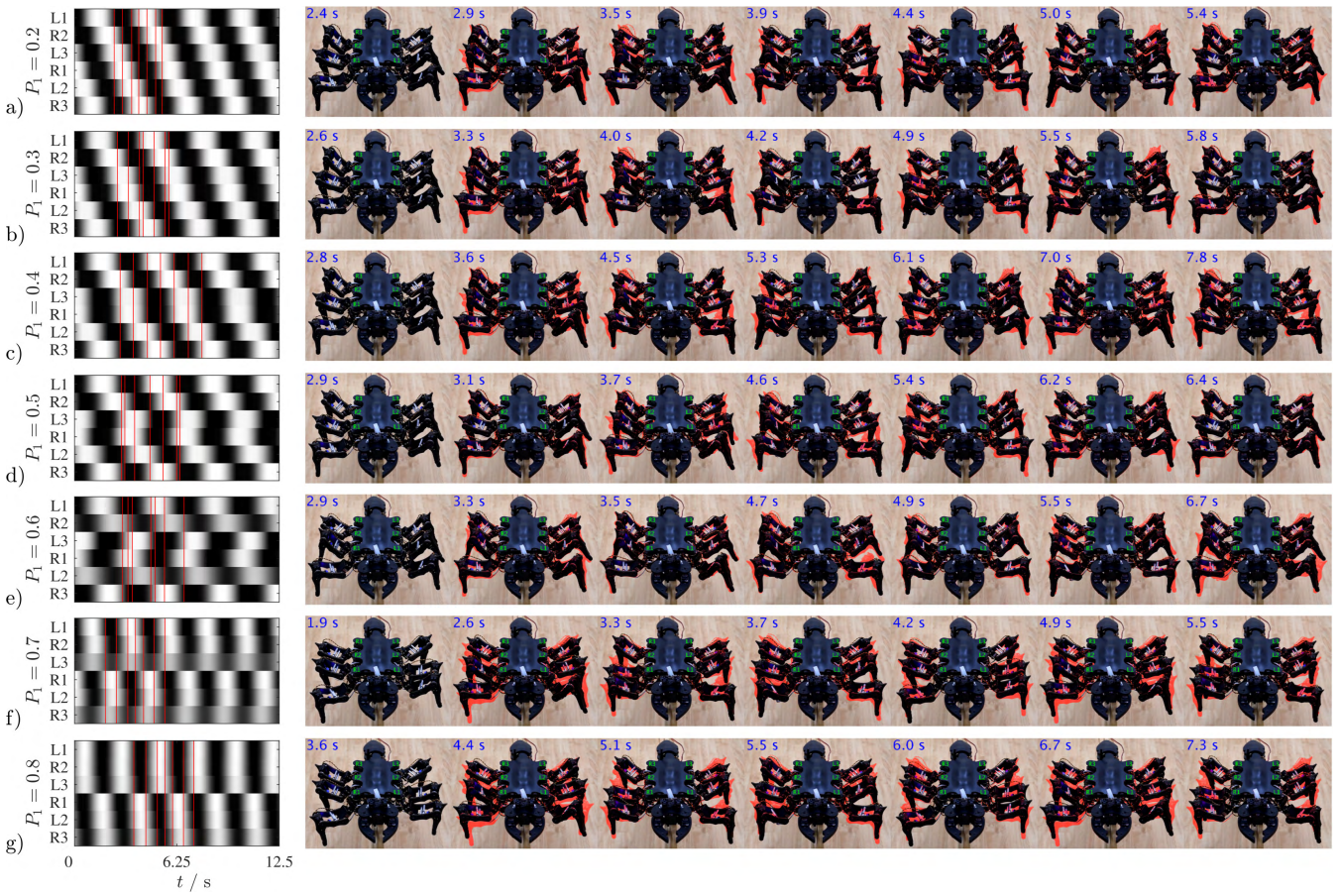

FIGURE 6. **Representative gaits obtained as a function of the gait selection parameter P_1, while setting $P_2 = P_3 = 1$ and $P_4 = P_5 = 0$, and corresponding frame sequences acquired with the suspended robot (i.e., legs not contacting terrain). a) Wave gait; b,d,e,f) Intermediate gaits; c) Tetrapod (metachronal) gait; g) Tripod gait. In the gait diagrams, representing the CPG output signals, black and white areas respectively denote the swing and stance phases, and the frame times are indicated by red bars. The red halo in each frame represents the robot posture in the previous frame shown. CPG: Central Pattern Generator. Corresponding video files available online [36].**

delineated clear convergence to different limit cycles after initial transient stabilization. By contrast, the trajectory for the case of uncoordinated movement, visible in Fig. 9c had a significantly more complex structure, which was unrelated to CPG output and resembled a strange attractor; however, convincing signatures of self-similarity could not be detected upon calculation of the local slopes of the correlation sum (correlation dimension analysis as in [26]; data not shown). The femur strain signals $\varepsilon_i(t)$ corresponding to these cases, shown in Fig. 7f, Fig. 8f and Fig. 9f, revealed markedly lower regularity under the condition of uncoordinated movement compared to the other two; it should be noted that, within each experimental run, the time-course differences between legs reflected multiple factors such as the weight distribution on the robot and the controller parameter settings.

Further emergent features of the gaits could be garnered by considering the pitch $\theta(t)$, roll $\phi(t)$ and the body elevation over terrain $\hat{z}(t)$ (where $\hat{}$ denotes world frame coordinate). Considering the variances of pitch and roll, i.e. $\sigma^2[\theta(t)]$ and $\sigma^2[\phi(t)]$, as measures of kinematic stability, it was observed that walking in the ant-like posture was generally more stable, particularly for the tripod gait (e.g., Fig. 7g), and primarily associated with pitch oscillation, whereas walking in the cockroach-like posture was associated to larger roll oscillation regardless of the gait (e.g., Fig. 8g). We additionally observed that, compared to the situation for the slower wave and tetrapod gaits, walking in the faster tripod gait and ant-like posture lead to the robot spontaneously adopting a more elevated position, plausibly also owing to a more even load distribution between the legs; the gradual emergence of this feature is well-evident in Fig. 7h. As expected, under the condition of uncoordinated movement, disordered attitude changes and particularly large pitch swings arose (Fig. 9g), accompanied by the largest observed instability of body elevation, manifest with the robot cyclically raising itself and falling back towards the ground as visible in Fig. 9h.

Consideration of the average longitudinal and transverse (i.e., forward and sideways) speeds in the body frame, referred to as $\delta x(t)$ and $\delta y(t)$, confirmed some features of the gaits in line with pre-established biological observations, namely that in the ant-like posture, the tripod gait delivered considerably faster locomotion than the wave and

TABLE 3. Summary of the experimental kinematic variables. Settings: P_1 gait selection parameter, P_2 activation parameter, P_3 CPG→LPGs coupling strength parameter, P_4 posture parameter, P_5 steering parameter. Measurements: τ gait period, η gait periodicity ratio (from the leg strains $\varepsilon_i(t)$), $\sigma^2[\theta(t)]$ pitch variance, $\sigma^2[\phi(t)]$ roll variance, $\langle\hat{z}(t)\rangle$ average elevation over terrain, $\langle\delta x(t)\rangle$ average longitudinal speed (body frame), $\langle\delta y(t)\rangle$ average transverse speed (body frame), $\langle\delta\Psi(t)\rangle$ average yaw rate, Δt data length. "$\emptyset$" denotes absence of sustained motion, "$\forall$" an irrelevant setting. Each row represents a distinct experimental run n; runs denoted with "*" are repetitions, which were performed to evaluate repeatability. Corresponding data files available online [36].

n	P_1	P_2	P_3	P_4	P_5	τ/s	η	$\sigma^2[\theta(t)]$ /deg^2	$\sigma^2[\phi(t)]$ /deg^2	$\langle\hat{z}(t)\rangle$ /mm	$\langle\delta x(t)\rangle$ /(mm s^{-1})	$\langle\delta y(t)\rangle$ /(mm s^{-1})	$\langle\delta\Psi(t)\rangle$ /(deg s^{-1})	Δt/s
Ant-like posture, walking straight														
1	0.2	1	1	0	0	2.94	0.96	6.87	3.52	57.1	28.9	4.6	0.93	105.9
2	0.3	1	1	0	0	3.12	0.89	5.50	3.34	57.8	26.7	3.7	1.01	100.2
3	0.4	1	1	0	0	3.38	0.91	7.14	3.34	64.7	22.5	2.7	0.89	105.1
4	0.5	1	1	0	0	3.38	0.89	12.60	7.75	69.6	33.0	1.6	-0.14	102.9
5	0.6	1	1	0	0	$\emptyset$	$\emptyset$	$\emptyset$	$\emptyset$	$\emptyset$	$\emptyset$	$\emptyset$	$\emptyset$	n/a
6	0.7	1	1	0	0	2.31	0.78	9.21	2.81	93.6	34.2	-0.1	1.26	89.2
7	0.8	1	1	0	0	2.31	0.91	7.32	2.88	93.9	49.6	-2.5	-0.14	92.9
8*	0.8	1	1	0	0	2.31	0.82	7.01	2.62	93.9	57.7	-8.0	-0.28	92.9
9*	0.8	1	1	0	0	2.31	0.88	7.27	2.25	95.1	48.6	-4.4	-0.86	94.7
Cockroach-like posture, walking straight														
10	0.2	1	1	1	0	2.94	0.92	1.22	15.43	72.8	24.0	-6.2	0.13	110.8
11*	0.2	1	1	1	0	2.94	0.94	0.51	13.40	67.2	23.4	-2.3	0.02	111.0
12*	0.2	1	1	1	0	2.94	0.93	0.65	15.81	68.7	19.2	0.5	-0.42	76.2
13	0.3	1	1	1	0	3.19	0.94	0.60	13.57	67.6	24.4	-0.9	0.01	111.7
14	0.4	1	1	1	0	3.31	0.90	0.78	13.64	65.6	20.4	-2.8	0.06	115.4
15	0.5	1	1	1	0	3.38	0.67	0.65	16.32	61.4	18.0	0.3	-0.19	109.7
16	0.6	1	1	1	0	$\emptyset$	$\emptyset$	$\emptyset$	$\emptyset$	$\emptyset$	$\emptyset$	$\emptyset$	$\emptyset$	n/a
17	0.7	1	1	1	0	2.31	0.75	1.13	13.60	70.1	15.4	-4.5	0.01	101.1
18	0.8	1	1	1	0	2.31	0.67	1.23	15.95	75.2	31.1	-3.7	-0.14	91.4
Ant-like posture, steering														
19	0.8	1	1	0	-1	2.31	0.89	2.45	2.64	95.0	28.0	18.2	7.19	94.7
20*	0.8	1	1	0	-1	2.31	0.86	3.67	2.49	89.1	27.7	13.6	6.41	95.1
Uncoordinated movement														
21	$\forall$	1	0	0	0	4.44	0.55	13.17	4.12	66.6	3.1	-1.1	-0.01	120.8
22*	$\forall$	1	0	0	0	6.72	0.52	20.26	6.60	61.6	1.9	-1.3	0.11	115.1

intermediate gaits; in the cockroach-like posture, the differences between gaits were less marked and the speed was on average lower. The transverse speed, ideally zero, was always considerably lower than the longitudinal speed, i.e. $|\delta y(t)| \approx |\delta x(t)|/10$. As expected, for uncoordinated movement very limited effective locomotion was observed. Consideration of the yaw rate $\delta\Psi(t)$ further indicated that, besides relatively contained fluctuations, after stabilization of the initial transient all combinations of settings provided a straight trajectory, with the exception of the runs with non-zero steering parameter P_5, which successfully generated a continuous rotation of the body along the yaw axis.

These data confirm that all gaits and both postures provided effective locomotion. This was in spite of the fact that control was purely open-loop, namely there was no feedback to adjust posture, heading etc. The trajectories in world frame coordinates $\hat{x}$ and $\hat{y}$ corresponding to the cases considered above are shown in Fig. 7d, Fig. 8d and Fig. 9d.

It should nevertheless be noted that the repeated runs performed for four representative settings indicated that the repeatability of the kinematic measurements was incomplete: as reported in Table 3, the relative error was generally on the order of 10%, but at times reached substantially higher levels, particularly for transverse speed and rotation, especially when the corresponding values were small. A systematic reproducibility evaluation was out of scope for the present study, but given the high stability of the pattern generation ($\eta \approx 1$ as indicated above, and negligible variability of period τ), it appears plausible that the error was dominated by mechanical factors, particularly slippage of the feet against the floor due to the limited contact area.

IV. DISCUSSION

A. HIERARCHICAL ARCHITECTURE

Hexapod robots realistically modeling insects generally possess three degrees of freedom per leg, raising the challenge of translating each CPG output into multiple signals, suitable for driving the actuators coupled to the coxa-body, femur-coxa and tibia-femur joints [3]–[5], [8], [12]. In particular, physically realizing a given "global" gait pattern (representing the phase relationships between the legs) requires identifying a set of suitable "local" patterns (i.e., joint trajectories for the individual legs); this is a computational problem of considerable complexity, which insects appear to solve seamlessly when realizing the canonical gaits in a highly adaptive manner depending, for example, on surface roughness and inclination [1], [2].

In the majority of existing controllers, a non-hierarchical approach is used and the individual leg actuators are directly driven based on multiple outputs generated by each oscillator instanced in the CPG; for example, the coxa-body and femur-coxa joints can be mapped to the x and y outputs of each cell in a *cellular non-linear network*, while fixing the tibia-femur joint to a predetermined angle [4], [21], [34].

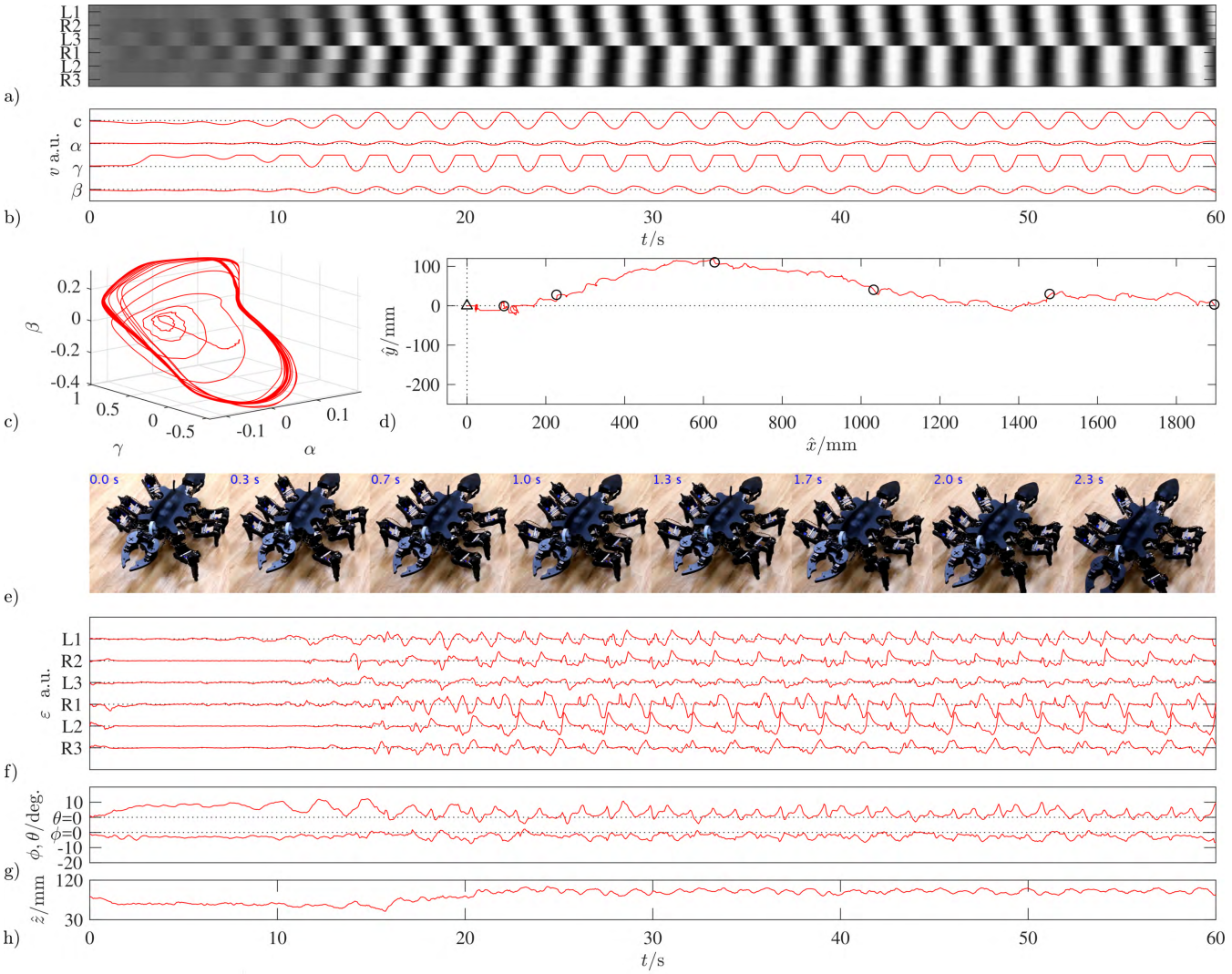

FIGURE 7. Experimental data acquired for walking according to the tripod gait, in the ant-like posture (run $n = 7$; $P_1 = 0.8$, $P_2 = P_3 = 1$ and $P_4 = P_5 = 0$). a) Gait diagram, representing the CPG output signals; black and white areas respectively denote the swing and stance phases. b) Example output signals from the CPG and LPG nodes of leg R1; the joints α, β and γ are specified in Fig. 5b. c) Corresponding leg trajectory in joint angles space [α, β, γ], arbitrary units. d) Robot trajectory in world frame coordinates $\hat{x}$ and $\hat{y}$; the triangle denotes starting location, the circles denote locations at 10 s intervals. e) Representative frame sequence, spanning approximately one gait period. f) Femur strain signals $\varepsilon_i(t)$. g) Pitch and roll signals $\theta(t)$ and $\phi(t)$. h) Body elevation over terrain signal $\hat{z}(t)$. CPG: Central Pattern Generator. LPG: Local Pattern Generator. Corresponding video and data files available online [36].

Some controllers are "hybrid" in that they include a bio-inspired CPG implemented in the form of a circuit, but the translation of its outputs into leg actuator signals is achieved by means of conventional robotics techniques, namely inverse kinematic modeling [43], [44]. Other controllers simply implement linear mapping between the CPG outputs and the leg joints [45]. To the authors' knowledge, only a minority of studies have realized truly hierarchical controllers, wherein each leg is associated to a local network of nodes which receive the corresponding CPG input and process it in a non-linear manner depending on additional parameters [22], [46], [47].

In this work, a fully hierarchical approach was adopted, wherein each leg is associated to a ring-like structure comprising three nodes that effectively constitute a distinct pattern generator, driven by the corresponding CPG node to which it is unidirectionally coupled. This level of complexity was instrumental to attaining the demonstrated level of flexibility, for example by making it possible to seamlessly shift between two completely different locomotion schemes (or postures), one wherein the power stroke is exclusively delivered by the coxa-body joints and another wherein the same is primarily delivered by the tibia-femur joints.

It is also noteworthy that, in comparison to some of the other hierarchical controllers cited above, the present network was appreciably smaller and therefore more suitable for physical implementation as an analog circuit. As previously mentioned, even though VLSI- and FPGA-based CPG implementations have been proposed, to the authors' knowledge this is also the first FPAA-based implementation of a

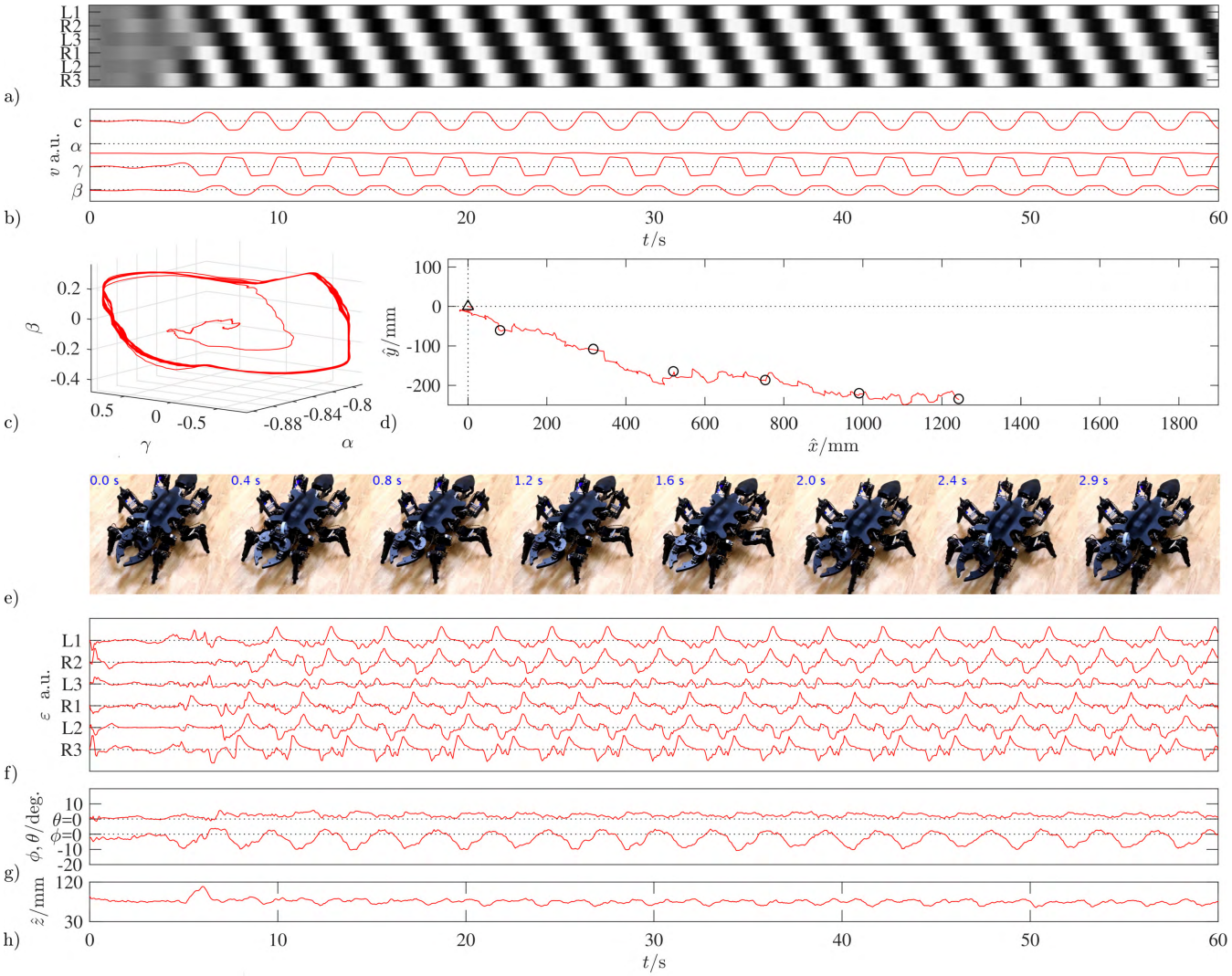

FIGURE 8. Experimental data acquired for walking according to the wave gait, in the cockroach-like posture (run $n = 10$; $P_1 = 0.2$, $P_2 = P_3 = P_4 = 1$ and $P_5 = 0$). a) Gait diagram, representing the CPG output signals; black and white areas respectively denote the swing and stance phases. b) Example output signals from the CPG and LPG nodes of leg R1; the joints α, β and γ are specified in Fig. 5b. c) Corresponding leg trajectory in joint angles space [α, β, γ], arbitrary units. d) Robot trajectory in world frame coordinates $\hat{x}$ and $\hat{y}$; the triangle denotes starting location, the circles denote locations at 10 s intervals. e) Representative frame sequence, spanning approximately one gait period. f) Femur strain signals $\varepsilon_i(t)$. g) Pitch and roll signals $\theta(t)$ and $\phi(t)$. h) Body elevation over terrain signal $\hat{z}(t)$. CPG: Central Pattern Generator. LPG: Local Pattern Generator. Corresponding video and data files available online [36].

complete CPG; in the area of bio-inspired robotics, custom FPAAs have previously been used only for robot trajectory planning and to implement a leaky-integrate-and-discharge type oscillator [27], [48], [49].

Another notable feature of the proposed controller is the presence of a coupling strength parameter explicitly setting how tightly the LPG dynamics are driven by the CPG, i.e. "extrinsic", as opposed to internally-generated independently of the CPG, i.e. "intrinsic". Low values of this parameter lead to desynchronization, visible in the form of uncoordinated movement resembling, at least at the surface, thrashing as observed in insects during some forms of neuroreceptor blockade (e.g., insecticide poisoning), or during attempts to become untrapped [1], [2]. A similar capability is also present in other circuits based on chaos control, but the difference is that in such cases the transition to chaos is driven by absence or alteration of environmental feedback to the CPG, whereas in the present case it is internally managed by a specific parameter [22]. The ability to selectively decouple the activity of individual legs from the CPG (not explicitly demonstrated in study, but clearly implied in the architecture of the controller) can provide a richer framework to study failure compensation compared to the situation wherein a leg is entirely disabled (e.g., effectively amputated), as was done for chaos-based control in [47].

B. GENERALIZED GAIT

The notion of a generalized gait introduced in [34] was implemented with recourse to three sigmoidal membership functions peaking at low, mid and high values of a single gait

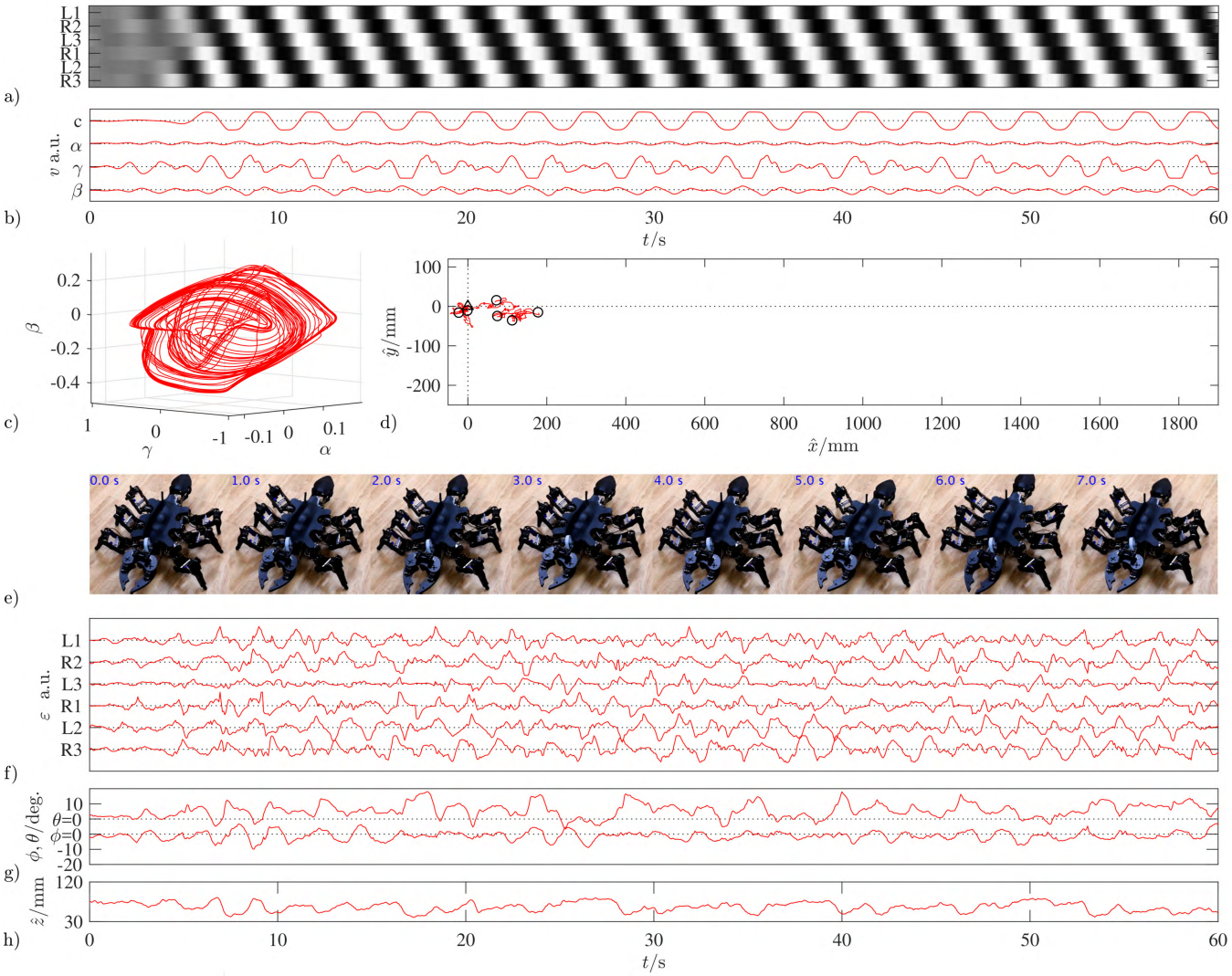

FIGURE 9. Experimental data for uncoordinated movement (run $n = 22$; $P_1 = 0.2$, $P_2 = 1$, $P_3 = P_4 = P_5 = 0$). a) Gait diagram, representing the CPG output signals, which are irrelevant in this case since the LPGs were uncoupled. b) Example output signals from the CPG and LPG nodes for leg R1; the joints α, β and γ are specified in Fig. 5b. c) Corresponding leg trajectory in joint angles space [α, β, γ], arbitrary units. d) Robot trajectory in world frame coordinates $\hat{x}$ and $\hat{y}$; the triangle denotes starting location, the circles denote locations at 10 s intervals. e) Representative frame sequence, spanning approximately 7 s. f) Femur strain signals $\varepsilon_i(t)$. g) Pitch and roll signals $\theta(t)$ and $\phi(t)$. h) Body elevation over terrain signal $\hat{z}(t)$. CPG: Central Pattern Generator. LPG: Local Pattern Generator. Corresponding video and data files available online [36].

selection parameter, following principles similar to those of neuro-fuzzy membership. As discussed above, depending on this parameter the CPG produces a variety of gaits including not only the ''canonical'' wave, tetrapod (or metachronal) and tripod gaits but also a number of intermediate ones [1], [2], [4], [34]. Besides gait selection, the activation parameter was provisioned to allow enabling and inhibiting the CPG, and even obtaining approximate reverse patterns. It was demonstrated that the CPG responds satisfactorily to both gradual and step changes of the gait selection parameter, effectively setting walking speed, as well as to step changes of the activation parameter. In a practical application such parameters would be controlled dynamically, i.e. as $P_1(t) \ldots P_5(t)$, by a system playing the role of higher-level areas to purposefully drive the robot. Another noteworthy aspect of the proposed controller is that the discrete-time implementation based on switched-capacitor circuits ensures that all parameters are effectively orthogonal to the clock rate; as a consequence, the frequency at which a given gait is generated can be controlled completely independently of all other parameters, effectively decoupling gait and locomotion speed.

As expected and summarized in Table 3, there were several differences between the gaits and postures. The tripod gait (high P_1), commonly observed in insects in association with fast locomotion for example during escape, accordingly provided maximum speed [1], [2]; its period was spontaneously lower than that of the wave gait and intermediate gaits, representing an emergent property since no time constant or filter frequency parameters were altered, only the connectivity

pattern was changed. This gait provided the highest speed and best stability, according to both pitch/roll variance and femural strains, when reproduced in the ant-like posture, which also spontaneously resulted in a higher body elevation. Contrariwise, the wave gait (low P_1), commonly observed in insects in association to situations requiring slow locomotion such as foraging [1], [2], provided the lowest speed and had more similar stability between the two postures, with the exception of greater roll in the cockroach-like posture. Uncoordinated movement resulted in the most irregular femural strain signals, very limited locomotion and highest pitch variance, even though rolling was smaller compared to the cockroach-like posture. These results highlight the viability of the controller in a wide range of configurations. It should be noted, however, that the observed kinematic differences reflect not only emergent features of the controller network itself, but are also the result of the characteristics of the robot mechanics (e.g. weight distribution, maximum joint torque etc.) and of the values assigned to the large number of constant parameters specified in Tables 4 and 6.

C. ROLE OF THE NON-LINEARITY

Recent work has shown that chaotic oscillators harbor substantial potential for bio-inspired robotics, in that they allow generating a broad range of gait patterns depending on a single control parameter, under the assumption that feedback from the environment is available [22], [43], [47]. In the initial study where our oscillator was introduced, an extended region of the control parameter space was explored aiming to obtain periodic and chaotic collective oscillation of a ring network, and in particular to elicit the phenomenon of remote synchronization, which occurs close to the transition between the two phases [26]. Here, however, the non-linear oscillator operated in a very different region and frequency band, and neither transition to chaos nor bifurcations were observed. In other words, the non-linear nature of the oscillator was simply exploited to obtain different stable limit cycles and phase relationships, unlike for example [22] where it played a deeper generative role.

Rather than being fully emergent from the dynamics, the transitions between the canonical gaits were for the most part directly driven by the connectivity pattern under the influence of the gait selection parameter; in this sense, the present controller is more founded on synchronization patterns than on the dynamical properties of the individual oscillators. However, additional emergent gaits were also observed. Furthermore, emergent signatures of non-linear dynamics were nevertheless observed around the point of transition between the wave-like gaits and the tripod gait, i.e. for $P_1 \approx 0.6$: at that point, the transition between the two gaits was clearly hysteretic, hence a first-order one. In the same region, disordered patterns could be generated, breaking the periodicity observed for the regular gait patterns, and metastability was also evident. These results are noteworthy as they closely recall observations of gait transitions in insects and other animal species [38], [50].

D. REMARKS ON PERFORMANCE

Unbiased performance comparison between CPG-based controllers is presently complicated by the diversity of approaches and absence of standardized criteria, nevertheless it is appropriate to further juxtapose the proposed controller with the existing literature in this regard.

First, compared to the initial works wherein the notion of generalized gait was introduced, the proposed controller offers similar or superior capability as regards the range of canonical and intermediate gaits which can be generated, with the added advantage that gait selection is controlled by a single parameter [4], [34]. Compared to chaos-based controllers, the diversity of gaits also appears overall comparable, however it should be noted that the present controller did not generate separate slow and fast wave gaits [22]. It is also noteworthy that the gait summary parameter ζ introduced in the present study has general usefulness for evaluating and comparing gait-generating architectures.

Second, in terms of implementation of the generated gaits, by design the present controller has features which to the authors' knowledge are unique in literature, in that its hierarchical architecture delivers a notable level of posture and coordination versatility, because the operation of the CPG and that of the LPGs are both parameterized.

Third, in terms of adaptiveness with respect to walking over slopes and irregular terrains, existing controllers predicated on connectionist and chaos-control approaches are remarkably successful [17], [19], [22], [44], [51]. Assessing the performance of the present architecture in this regard was beyond the scope of the work. Furthermore, standardized testing conditions and measures for comparing this aspect of performance are yet to be defined.

Fourth, external controllability, intended as the ability to purposefully alter activity via changing parameter settings, has also been extensively demonstrated for connectionist and chaos-control approaches, and the characteristics of the present controller appear in line with existing literature [4], [22], [34]. However, given the diversity of approaches there is again no consensus regarding the testing conditions, and future work should explicitly compare the available controllers in terms of latency and stability in response to control parameter changes.

Fifth, in terms of stability of the intrinsically-generated gait patterns, the available literature offers largely anecdotal evidence in the form of illustrations rather than quantitative measurements (e.g. [4]). In the present study a measure of periodicity, the periodicity ratio η, was introduced and allowed explicitly confirming the high stability of controller output.

Sixth, in terms of ability to drive a physical robot in a kinematically-stable manner, to the authors' knowledge no comprehensive evaluations have as yet been performed. A prerogative of the present study is that the issue was addressed explicitly via telemetry of body rotations and structural strains. The results indicate a moderate level of stability where, as previously discussed, certain combinations of gaits

TABLE 4. Hardwired LPG node input connectivity and corresponding weights (i.e., input gains) for each LPG node. The gains G_1, G_2 and G_3 are determined by parameters P_3 and P_4, which are high-level settings as specified in Table 1; $B_1 \ldots B_9$ are constants, see text for description. Voltages v_L and v_C denote the two external inputs of each node, one connected to another node in the same LPG and the other to the CPG node which drives the LPG, and weighted respectively by the gains G_1 and G_2; G_3 determines the loop gain within each node (see Figs. 3b and c). For succinctness, $P'_3 = 1 - P_3$ and $P'_4 = 1 - P_4$. CPG: Central Pattern Generator. LPG: Local Pattern Generator.

For node	v_L	v_C	G_1	G_2	G_3
L1/α	$-4v_{2,L1/\gamma}$	$v_{5,L1/C}$	$B_1 P'_3$	P_3	$B_2 P'_3 + B_3 P_3 P'_4$
R2/α	$-4v_{2,R2/\gamma}$	$v_{5,R2/C}$	$B_1 P'_3$	P_3	$B_2 P'_3 + B_3 P_3$
L3/α	$-4v_{2,L3/\gamma}$	$v_{5,L3/C}$	$B_1 P'_3$	P_3	$B_2 P'_3 + B_3 P_3 P'_4$
R1/α	$-4v_{2,R1/\gamma}$	$v_{5,R1/C}$	$B_1 P'_3$	P_3	$B_2 P'_3 + B_3 P_3 P'_4$
L2/α	$-4v_{2,L2/\gamma}$	$v_{5,L2/C}$	$B_1 P'_3$	P_3	$B_2 P'_3 + B_3 P_3$
R3/α	$-4v_{2,R3/\gamma}$	$v_{5,R3/C}$	$B_1 P'_3$	P_3	$B_2 P'_3 + B_3 P_3 P'_4$
L1/β	$-v_{5,L1/\alpha}$	$v_{5,L1/C}$	$-P'_3$	$P_3(1 + B_4 P_4)$	$B_5 P_3 P_4$
R2/β	$-v_{5,R2/\alpha}$	$v_{5,R2/C}$	$-P'_3$	P_3	0
L3/β	$-v_{5,L3/\alpha}$	$v_{5,L3/C}$	$-P'_3$	$P_3(1 + B_4 P_4)$	$B_5 P_3 P_4$
R1/β	$-v_{5,R1/\alpha}$	$v_{5,R1/C}$	$-P'_3$	$P_3(1 + B_4 P_4)$	$B_5 P_3 P_4$
L2/β	$-v_{5,L2/\alpha}$	$v_{5,L2/C}$	$-P'_3$	P_3	0
R3/β	$-v_{5,R3/\alpha}$	$v_{5,R3/C}$	$-P'_3$	$P_3(1 + B_4 P_4)$	$B_5 P_3 P_4$
L1/γ	$-4v_{2,L1/\beta}$	$v_{5,L1/C}$	$B_6 P'_3 + B_7 P_3 P'_4$	$-B_8 P_3 P_4$	$B_9 P_3 P'_4$
R2/γ	$-4v_{2,R2/\beta}$	$v_{5,R2/C}$	$B_6 P'_3 + B_7 P_3$	0	$B_9 P_3$
L3/γ	$-4v_{2,L3/\beta}$	$v_{5,L3/C}$	$B_6 P'_3 + B_7 P_3 P'_4$	$B_8 P_3 P_4$	$B_9 P_3 P'_4$
R1/γ	$-4v_{2,R1/\beta}$	$v_{5,R1/C}$	$B_6 P'_3 + B_7 P_3 P'_4$	$-B_8 P_3 P_4$	$B_9 P_3 P'_4$
L2/γ	$-4v_{2,L2/\beta}$	$v_{5,L2/C}$	$B_6 P'_3 + B_7 P_3$	0	$B_9 P_3$
R3/γ	$-4v_{2,R3/\beta}$	$v_{5,R3/C}$	$B_6 P'_3 + B_7 P_3 P'_4$	$B_8 P_3 P_4$	$B_9 P_3 P'_4$

and postures are highly viable whereas others were reproduced sub-optimally. Standardized testing conditions and measures are again lacking and an explicit comparison of the existing approaches would represent an important future contribution. In this regard, the present approach, which involved calculating the periodicity ratio η from the leg strains $\varepsilon_i(t)$ and considering it in conjunction with the pitch and roll variances $\sigma^2[\theta(t)]$ and $\sigma^2[\phi(t)]$, may have general value.

Lastly, the walking speed of the robot was on the order of 0.02 m/s to 0.06 m/s. While this value is strongly influenced by mechanical aspects and parameter settings and thus not truly representative of controller performance, we note that it is overall comparable with other hexapod robots driven by bio-inspired controllers. In particular, it closely overlaps experimental measurements of controllers based on connectionist approaches (e.g., 0.03 m/s to 0.05 m/s in [4]); however, compared to some experiments with chaos-based controllers the maximum speed was lower and the difference between the fastest and slowest gaits was accordingly more constrained (e.g., 0.03 m/s to 0.14 m/s in [22]).

E. DIRECTIONS FOR FUTURE RESEARCH

Since the proposed controller is inherently well-suited for rapid and ongoing reconfiguration, future work will leverage this capability. For example, several previous studies have demonstrated the possibility of delivering stable locomotion, heading and attitude even in presence of instabilities and tolerances in the actuators and mechanics, irregular surfaces and slopes, by means of suitable feedback signals, and attempts should be made to replicate such results using the proposed controller [17], [19], [44], [51]. In fact, maneuverability over irregular terrain is one of the primary strengths of hexapod robots compared to rovers, and the main limitation of this initial study is that the controller was only demonstrated in an open-loop configuration, which inherently prohibits locomotion in presence of irregularities or obstacles. Addressing this important issue will likely require the introduction of additional parameters beyond the five ones considered in this study, to be adjusted based on inertial data and terrain contact feedback, allowing controlling pitch and roll independently of all other aspects; since Tables 4 and 6 contain all information required to map the CPG outputs to the corresponding legs, such additional parameters will enter the expressions contained in these tables. Furthermore, it should be noted that the constant values set in this initial study were chosen empirically and as such may require optimization for improved performance; this could be attained, for example, using genetic algorithms as previously done in [18].

To realize more complex and realistic behaviors the high-level control parameters $P_1 \ldots P_5$, rather than being statically set for each experimental run, should be driven dynamically as $P_1(t) \ldots P_5(t)$ by afferences from "higher" circuits capable, for example, of exhibiting learning based on the delivery of reward such as in [52], and of performing purposeful tasks based on visual and other multisensory input such as in [43], [46], and [53].

A controller such as the present one, wherein significant versatility is condensed into a handful of parameters, also has inherent potential in the field of brain-computer and brain-machine interfaces, wherein usability is knowingly inversely related to the number of commands and variables that need to be decoded [54]. Importantly, the present work allows control in a seamless, continuous manner, without necessitating the decoding of discrete commands, and as such may have specific advantages in terms of operability and learning curve compared to more traditional interfaces [55]. Future research will therefore include real-time control with ongoing decoding of all or a subset of the five parameters from

TABLE 5. Description of the B parameters, which influence LPG node input connectivity as specified in Table 4. LPG: Local Pattern Generator.

Parameter	Control target	Applicable configuration(s)	Target legs	Target joints
B_1	Within-LPG $\gamma \rightarrow \alpha$ coupling	Uncoordinated movement	All	α
B_2	Internal loop gain	Uncoordinated movement	All	α
B_3	Internal loop gain	Walking in ant-like (front, hind legs) or any posture (middle legs)	All	α
B_4	CPG→LPG coupling	Walking in cockroach-like posture	Front and hind	β
B_5	Internal loop gain	Walking in cockroach-like posture	Front and hind	β
B_6	Within-LPG $\beta \rightarrow \gamma$ coupling	Uncoordinated movement	All	γ
B_7	Within-LPG $\beta \rightarrow \gamma$ coupling	Walking in ant-like (front, hind legs) or any posture (middle legs)	All	γ
B_8	CPG→LPG coupling	Walking in cockroach-like posture	Front and hind	γ
B_9	Internal loop gain	Walking in ant-like (front, hind legs) or any posture (middle legs)	All	γ

electroencephalographic signals or other bio-signals, implemented for instance by means of directly mapping power density at specific sites or cortical regions to the parameters, or with recourse to sparse activity representations [56].

V. CONCLUDING REMARKS

This work aimed to address the issues of flexibility and availability associated with implementing CPGs by means of custom integrated circuits. A novel CPG network wherein each node is an FPAA-based oscillator was introduced. Besides its inherent flexibility, the controller features a hierarchical architecture which confers a high level of versatility in gait, posture and coordination. It was demonstrated that the resulting large number of low-level parameters can be handled through constructing the corresponding expressions as the superposition of a minimal number of canonical gaits and postures, as specified via five high-level parameters. The controller was deployed to a physical robot, and in order to confirm its viability, a range of experimental measures were considered, which also warrant future consideration as means of comparing controllers in this area.

APPENDIX

As for determination of the single oscillator parameters, given the absence of a formal approach we proceeded iteratively for the B parameters, specified in Table 4 and further described in Table 5, in the following manner. First, we considered only the case of extrinsic activity ($P_3 = 1$) and thus fixed $B_1 = B_2 = B_6 = 0$: 1) given the ant-like posture ($P_4 = 0$), in which all legs operate identically, we fixed $B_4 = B_5 = B_8 = 0$ and adjusted B_3, B_7 and B_9 in order to obtain robust synchronization and the phase relationships between the α, β and γ outputs necessary to implement viable leg trajectories (examples of which can be found in [4]), 2) given the cockroach-like posture ($P_4 = 1$), we then adjusted B_4, B_5 and B_8 to obtain the desired differentiation for the front and hind legs, 3) because parameters B_3, B_7 and B_9 affect both postures, they had to be iteratively adjusted trying to find settings acceptable for both. In steps 1) and 2) each free parameter was initially set to either 1 or -1, then adjusted. Second, we considered the case of intrinsic activity ($P_3 = 0$) and adjusted B_1, B_2 and B_6 until sustained leg swings were elicited, with features similar to the circle-like movements observed biologically. As the C parameters were not yet defined, these steps were completed with the controller network deployed on the physical hardware, but evaluating signal plots rather than materially driving the robot.

TABLE 6. Output gains for LPG to servo-motor connectivity (see Figs. 3b and c). The gains G_4 and G_5 are determined by parameters P_3, P_4 and P_5, which are high-level settings as specified in Table 1; $C_1 \ldots C_{29}$ are constants, see text for description. For succinctness, $P'_3 = 1 - P_3$, $P'_4 = 1 - P_4$, $P'_5 = 1 - R(-P_5)$ and $P''_5 = 1 - R(P_5)$, where $R(x)$ is the ramp function. LPG: Local Pattern Generator.

For node	G_4	G_5
L1/α	$C_1 P_3 P_4$	$C_2 P'_3 + C_3 P_3 P'_4 P''_5$
R2/α	0	$C_{12} P'_3 + C_{13} P_3 P''_5$
L3/α	$C_{19} P_3 P_4$	$C_{20} P'_3 + C_{21} P_3 P'_4 P'_5$
R1/α	$C_1 P_3 P_4$	$C_2 P'_3 + C_3 P_3 P'_4 P''_5$
L2/α	0	$C_{12} P'_3 + C_{13} P_3 P'_5$
R3/α	$C_{19} P_3 P_4$	$C_{20} P'_3 + C_{21} P_3 P'_4 P''_5$
L1/β	$C_4 P'_3 + C_5 P_3 P'_4$	$C_6 P'_3 + C_7 P_3 P_4 P'_5$
R2/β	C_{14}	$C_{15} P'_3$
L3/β	$C_{22} P'_3 + C_{23} P_3 P'_4$	$C_{24} P'_3 + C_{25} P_3 P_4 P'_5$
R1/β	$C_4 P'_3 + C_5 P_3 P'_4$	$C_6 P'_3 + C_7 P_3 P_4 P''_5$
L2/β	C_{14}	$C_{15} P'_3$
R3/β	$C_{22} P'_3 + C_{23} P_3 P'_4$	$C_{24} P'_3 + C_{25} P_3 P_4 P''_5$
L1/γ	$C_8 P'_3 + C_9 P_3 P'_4 + C_{10} P_3 P_4$	$C_{11} P'_3$
R2/γ	$C_{16} P'_3 + C_{17} P_3$	$C_{18} P'_3$
L3/γ	$C_{26} P'_3 + C_{27} P_3 P'_4 + C_{28} P_3 P_4$	$C_{29} P'_3$
R1/γ	$C_8 P'_3 + C_9 P_3 P'_4 + C_{10} P_3 P_4$	$C_{11} P'_3$
L2/γ	$C_{16} P'_3 + C_{17} P_3$	$C_{18} P'_3$
R3/γ	$C_{26} P'_3 + C_{27} P_3 P'_4 + C_{28} P_3 P_4$	$C_{29} P'_3$

As regards the C parameters, specified in Table 6 and further described in Table 7, we proceeded in a similar sequence. First, we considered only the case of extrinsic activity ($P_3 = 1$) and thus fixed $C_2 = C_4 = C_6 = C_8 = C_{11} = C_{12} = C_{15} = C_{16} = C_{18} = C_{20} = C_{22} = C_{24} = C_{26} = C_{29} = 0$: 1) given the ant-like posture ($P_4 = 0$), we further fixed $C_1 = C_7 = C_{10} = C_{19} = C_{25} = C_{28} = 0$ and adjusted C_3, C_5, C_9, C_{13}, C_{14}, C_{17}, C_{21}, C_{23} and C_{27} in order to obtain adequate swing on all leg axes, 2) given the cockroach-like posture ($P_4 = 1$), we then adjusted C_1, C_7, C_{10}, C_{19}, C_{25} and C_{28} to obtain adequate power stoke delivery with the front and hind legs, 3) because C_{13}, C_{14} and C_{17} affect both postures, they had to be iteratively adjusted trying to find settings acceptable for both. Second, we considered the case of intrinsic activity ($P_3 = 0$) and adjusted C_2, C_4, C_6, C_8, C_{11}, C_{12}, C_{15}, C_{16}, C_{18}, C_{20}, C_{22}, C_{24}, C_{26} and C_{29} until the corresponding movements were performed adequately. These steps were completed first observing the movement of individual legs with the robot suspended and making no terrain contact, then observing actual walking.

TABLE 7. Description of the *C* parameters, which influence LPG to servo-motor connectivity as specified in Table 6. LPG: Local Pattern Generator.

Parameter	Control target	Applicable configuration(s)	Target legs	Target joints
C_1	Position offset	Walking in cockroach-like posture	Front	α
C_2	Coupling coefficient for LPG direct output	Uncoordinated movement	Front	α
C_3	Coupling coefficient for LPG direct output	Walking in ant-like posture	Front	α
C_4	Coupling coefficient for LPG mixed output	Uncoordinated movement	Front	β
C_5	Coupling coefficient for LPG mixed output	Walking in ant-like posture	Front	β
C_6	Coupling coefficient for LPG direct output	Uncoordinated movement	Front	β
C_7	Coupling coefficient for LPG direct output	Walking in cockroach-like posture	Front	β
C_8	Coupling coefficient for LPG mixed output	Uncoordinated movement	Front	γ
C_9	Coupling coefficient for LPG mixed output	Walking in ant-like posture	Front	γ
C_{10}	Coupling coefficient for LPG mixed output	Walking in cockroach-like posture	Front	γ
C_{11}	Coupling coefficient for LPG direct output	Uncoordinated movement	Front	γ
C_{12}	Coupling coefficient for LPG direct output	Uncoordinated movement	Middle	α
C_{13}	Coupling coefficient for LPG direct output	Walking in any posture	Middle	α
C_{14}	Coupling coefficient for LPG mixed output	All	Middle	β
C_{15}	Coupling coefficient for LPG direct output	Uncoordinated movement	Middle	β
C_{16}	Coupling coefficient for LPG mixed output	Uncoordinated movement	Middle	γ
C_{17}	Coupling coefficient for LPG mixed output	Walking in any posture	Middle	γ
C_{18}	Coupling coefficient for LPG direct output	Uncoordinated movement	Middle	γ
C_{19}	Position offset	Walking in cockroach-like posture	Rear	α
C_{20}	Coupling coefficient for LPG direct output	Uncoordinated movement	Rear	α
C_{21}	Coupling coefficient for LPG direct output	Walking in ant-like posture	Rear	α
C_{22}	Coupling coefficient for LPG mixed output	Uncoordinated movement	Rear	β
C_{23}	Coupling coefficient for LPG mixed output	Walking in ant-like posture	Rear	β
C_{24}	Coupling coefficient for LPG direct output	Uncoordinated movement	Rear	β
C_{25}	Coupling coefficient for LPG direct output	Walking in cockroach-like posture	Rear	β
C_{26}	Coupling coefficient for LPG mixed output	Uncoordinated movement	Rear	γ
C_{27}	Coupling coefficient for LPG mixed output	Walking in ant-like posture	Rear	γ
C_{28}	Coupling coefficient for LPG mixed output	Walking in cockroach-like posture	Rear	γ
C_{29}	Coupling coefficient for LPG direct output	Uncoordinated movement	Rear	γ

Due to the large number of parameters and their interactions, the adjustment process was extremely labor intensive and required several weeks of experimental work. The above indications represent only general guidelines, and in practice a large number of adjustments were performed involving simultaneous tuning of both *B* and *C* parameters, aiming to maximize stability as well as kinematic realism; in particular, further tuning was needed to avoid ''tetanus'' due to competition between multiple configurations given intermediate settings of P_3 and P_4. It is due to this difficulty that other studies, even when gaits are generated by a CPG, almost universally resort to simple mappings or conventional kinematic models; while considerably less demanding to implement, such approaches are however also less biologically plausible [43]–[45].

ACKNOWLEDGEMENT

Realization of the hexapod robot hardware and related electronics was personally funded by L. Minati. In addition to employment by the Polish Academy of Sciences, Kraków, Poland, L. Minati gratefully acknowledges funding by the World Research Hub Initiative, Institute of Innovative Research, Tokyo Institute of Technology, Tokyo, Japan.

REFERENCES

[1] D. M. Wilson, ''Insect walking,'' *Annu. Rev. Entomol.*, vol. 11, no. 1, pp. 103–122, 1966.
[2] F. Delcomyn, ''Insect walking and robotics,'' *Annu. Rev. Entomol.*, vol. 49, no. 1, pp. 51–70, Jan. 2004.
[3] B. Webb, ''What does robotics offer animal behaviour?'' *Animal Behav.*, vol. 60, no. 5, pp. 545–558, Nov. 2000.
[4] M. Frasca, P. Arena, and L. Fortuna, *Bio-Inspired Emergent Control of Locomotion Systems*. Singapore: World Scientific, 2004.
[5] M. R. Clark, G. T. Anderson, and R. D. Skinner, ''Coupled oscillator control of autonomous mobile robots,'' *Auto. Robots.*, vol. 9, no. 2, pp. 189–198, Sep. 2000.
[6] M. Schilling, T. Hoinville, J. Schmitz, and H. Cruse, ''Walknet, a bio-inspired controller for hexapod walking,'' *Biol. Cybern.*, vol. 107, no. 4, pp. 397–419, Aug. 2013.
[7] H. Cruse, T. Kindermann, M. Schumm, J. Dean, and J. Schmitz, ''Walknet—A biologically inspired network to control six-legged walking,'' *Neural Netw.*, vol. 17, nos. 7–8, pp. 1435–1447, Oct. 1998.
[8] C. Ferrell, ''A comparison of three insect-inspired locomotion controllers,'' *Robot. Auto. Syst.*, vol. 16, nos. 2–4, pp. 135–159, Dec. 1995.
[9] U. Bässler, ''On the definition of central pattern generator and its sensory control,'' *Biol. Cybern.*, vol. 54, no. 1, pp. 65–69, May 1986.
[10] F. Delcomyn, ''Neural basis of rhythmic behavior in animals,'' *Science*, vol. 210, no. 4469, pp. 492–498, Oct. 1980.
[11] E. Marder and D. Bucher, ''Central pattern generators and the control of rhythmic movements,'' *Current Biol.*, vol. 11, no. 23, pp. 986–996, Nov. 2001.
[12] A. J. Ijspeert, ''Central pattern generators for locomotion control in animals and robots: A review,'' *Neural Netw.*, vol. 21, no. 4, pp. 642–653, 2008.
[13] J. Yu, M. Tan, J. Chen, and J. Zhang, ''A survey on CPG-inspired control models and system implementation,'' *IEEE Trans. Neural Netw. Learn. Syst.*, vol. 25, no. 3, pp. 441–456, Mar. 2014.
[14] A. Billard and A. J. Ijspeert, ''Biologically inspired neural controllers for motor control in a quadruped robot,'' in *Proc. IEEE-INNS-ENNS Int. Joint Conf. Neural Netw. (IJCNN)*, vol. 6. Jul. 2000, pp. 637–641.
[15] M. A. Lewis, R. Etienne-Cummings, M. J. Hartmann, Z. R. Xu, and A. H. Cohen, ''An in silico central pattern generator: Silicon oscillator, coupling, entrainment, and physical computation,'' *Biol. Cybern.*, vol. 88, no. 2, pp. 137–151, Feb. 2003.
[16] K. Matsuoka, ''Mechanisms of frequency and pattern control in the neural rhythm generators,'' *Biol. Cybern.*, vol. 56, no. 5, pp. 345–353, Jul. 1987.
[17] R. Campos, V. Matos, and C. Santos, ''Hexapod locomotion: A nonlinear dynamical systems approach,'' in *Proc. 36th Annu. Conf. IEEE Ind. Electron. Soc. (IECON)*, Glendale, AZ, USA, Nov. 2010, pp. 1546–1551.
[18] W. Li, W. Chen, X. Wu, and J. Wang, ''Parameter tuning of CPGs for hexapod gaits based on genetic algorithm,'' in *Proc. IEEE 10th Conf. Ind. Electron. Appl. (ICIEA)*, Auckland, New Zealand, Jun. 2015, pp. 45–50.

[19] P. Arena, L. Fortuna, and M. Frasca, "Attitude control in walking hexapod robots: An analogic spatio-temporal approach," *Int. J. Circuit Theory Appl.*, vol. 30, nos. 2–3, pp. 349–362, Mar. 2002.
[20] P. Arena and L. Fortuna, "Analog cellular locomotion control of hexapod robots," *IEEE Control Syst.*, vol. 22, no. 6, pp. 21–36, Dec. 2002.
[21] P. Arena, L. Fortuna, M. Frasca, and L. Patané, "A CNN-based chip for robot locomotion control," *IEEE Trans. Circuits Syst. I, Reg. Papers*, vol. 52, no. 9, pp. 1862–1871, Sep. 2005.
[22] S. Steingrube, M. Timme, F. Wörgötter, and P. Manoonpong, "Self-organized adaptation of a simple neural circuit enables complex robot behaviour," *Nature Phys.*, vol. 6, no. 3, pp. 224–230, Jan. 2010.
[23] A. Buscarino, L. Fortuna, M. Frasca, and G. Muscato, "Chaos does help motion control," *Int. J. Bifurcation Chaos*, vol. 17, no. 10, pp. 3577–3581, 2007.
[24] A. Pikovsky, M. Rosenblum, and J. Kurths, *Synchronization: A Universal Concept in Nonlinear Sciences*. Cambridge, U.K.: Cambridge Univ. Press, 2003.
[25] L. Minati, "Experimental synchronization of chaos in a large ring of mutually coupled single-transistor oscillators: Phase, amplitude, and clustering effects," *Chaos, Interdiscipl. J. Nonlinear Sci.*, vol. 24, no. 4, p. 043108, Dec. 2014.
[26] L. Minati, "Remote synchronization of amplitudes across an experimental ring of non-linear oscillators," *Chaos, Interdiscipl. J. Nonlinear Sci.*, vol. 25, no. 12, p. 123107, Dec. 2015.
[27] F. Li, A. Basu, C. H. Chang, and A. H. Cohen, "Dynamical systems guided design and analysis of silicon oscillators for central pattern generators," *IEEE Trans. Circuits Syst. I, Reg. Papers*, vol. 59, no. 12, pp. 3046–3059, Dec. 2012.
[28] Q. Chen, J. Wang, S. Yang, Y. Qin, B. Deng, and X. Wei, "A real-time FPGA implementation of a biologically inspired central pattern generator network," *Neurocomputing*, vol. 244, pp. 63–80, Jun. 2017.
[29] T. S. Hall, C. M. Twigg, J. D. Gray, P. E. Hasler, and D. V. Anderson, "Large-scale field-programmable analog arrays for analog signal processing," *IEEE Trans. Circuits Syst. I, Reg. Papers*, vol. 52, no. 11, pp. 2298–2307, Nov. 2005.
[30] E. Pierzchala, G. Gulak, L. Chua, and A. Rodríguez-Vázquez, *Field-Programmable Analog Arrays*. New York, NY, USA: Springer, 2013.
[31] A. Basu *et al.*, "A floating-gate-based field-programmable analog array," *IEEE J. Solid-State Circuits*, vol. 45, no. 9, pp. 1781–1794, Sep. 2010.
[32] E. K. F. Lee and P. G. Gulak, "A CMOS field-programmable analog array," *IEEE J. Solid-State Circuits*, vol. 26, no. 12, pp. 1860–1867, Dec. 1991.
[33] A. Buscarino, L. Fortuna, M. Frasca, and G. Sciuto, *A Concise Guide to Chaotic Electronic Circuits*. New York, NY, USA: Springer, 2014.
[34] P. Arena, L. Fortuna, M. Frasca, and G. Sicurella, "An adaptive, self-organizing dynamical system for hierarchical control of bio-inspired locomotion," *IEEE Trans. Syst., Man, Cybern. B Cybern.*, vol. 34, no. 4, pp. 1823–1837, Aug. 2004.
[35] *Understanding Anadigm Configurable Analog Modules (CAMs)*, Anadigm, Oak Park, CA, USA, Nov. 2002. [Online]. Available: http://www.anadigm.com/_apps/PR021100-0024.pdf
[36] *Publicly Available Data*. Accessed: Sep. 11, 2017. [Online]. Available: http://www.lminati.it/listing/2017/b/
[37] B. Boashash, "Estimating and interpreting the instantaneous frequency of a signal. II. Algorithms and applications," *Proc. IEEE*, vol. 80, no. 4, pp. 540–568, Apr. 1992.
[38] S. Fujiki, S. Aoi, T. Funato, N. Tomita, K. Senda, and K. Tsuchiya, "Hysteresis in the metachronal-tripod gait transition of insects: A modeling study," *Phys. Rev. E, Stat. Phys. Plasmas Fluids Relat. Interdiscip. Top.*, vol. 88, no. 1, p. 012717, Jul. 2013.
[39] J. A. Acebrón, L. L. Bonilla, C. J. P. Vicente, F. Ritort, and R. Spigler, "The Kuramoto model: A simple paradigm for synchronization phenomena," *Rev. Mod. Phys.*, vol. 77, no. 1, pp. 137–185, Apr. 2005.
[40] H. Hyyti and A. Visala, "A DCM based attitude estimation algorithm for low-cost MEMS IMUs," *Int. J. Navigat. Observ.*, vol. 2015, Nov. 2015, Art. no. 503814.
[41] H. Bay, A. Ess, T. Tuytelaars, and L. Van Gool, "SURF: Speeded up robust features," *Comput. Vis. Image Understand.*, vol. 110, no. 3, pp. 346–359, 2008.
[42] P. H. S. Torr and A. Zisserman, "MLESAC: A new robust estimator with application to estimating image geometry," *Comput. Vis. Image Understand.*, vol. 78, no. 1, pp. 138–156, 2000.
[43] P. Milička, P. Petr, and J. Faigl, "On chaotic oscillator-based central pattern generator for motion control of hexapod walking robot," in *Proc. CEUR Workshop ITAT*, vol. 1649. 2016, pp. 131–137.
[44] W. Chen, G. Ren, J. Wang, and D. Liu, "An adaptive locomotion controller for a hexapod robot: CPG, kinematics and force feedback," *Sci. China Inf. Sci.*, vol. 57, no. 11, pp. 1–18, Nov. 2014.
[45] H. Yu, W. Guo, J. Deng, M. Li, and H. Cai, "A CPG-based locomotion control architecture for hexapod robot," in *Proc. IEEE/RSJ Int. Conf. Intell. Robots Syst.*, Tokyo, Japan, Nov. 2013, pp. 5615–5621.
[46] L. A. Fuente, M. A. Lones, A. P. Turner, L. S. Caves, S. Stepney, and A. M. Tyrrell, "Adaptive robotic gait control using coupled artificial signalling networks, hopf oscillators and inverse kinematics," in *Proc. IEEE Congr. Evol. Comput.*, Cancun, Mexico, Jun. 2013, pp. 1435–1442.
[47] G. Ren, W. Chen, S. Dasgupta, C. Kolodziejski, F. Wörgötter, and P. Manoonpong, "Multiple chaotic central pattern generators with learning for legged locomotion and malfunction compensation," *Inf. Sci.*, vol. 294, pp. 666–682, Feb. 2015.
[48] S. Koziol, P. Hasler, and M. Stilman, "Robot path planning using field programmable analog arrays," in *Proc. IEEE Int. Conf. Robot. Autom.*, Saint Paul, MN, USA, May 2012, pp. 1747–1752.
[49] S. Koziol, R. Wunderlich, J. Hasler, and M. Stilman, "Single-objective path planning for autonomous robots using reconfigurable analog VLSI," *IEEE Trans. Syst., Man., Cybern., Syst.*, vol. 47, no. 7, pp. 1301–1314, Jul. 2017.
[50] J. J. Collins and I. Stewart, "Hexapodal gaits and coupled nonlinear oscillator models," *Biol. Cybern.*, vol. 68, no. 4, pp. 287–298, Feb. 1993.
[51] Y. Ambe, T. Nachstedt, P. Manoonpong, F. Wörgötter, S. Aoi, and F. Matsuno, "Stability analysis of a hexapod robot driven by distributed nonlinear oscillators with a phase modulation mechanism," in *Proc. IEEE/RSJ Int. Conf. Intell. Robots Syst.*, Tokyo, Japan, Nov. 2013, pp. 5087–5092.
[52] E. Arena, P. Arena, R. Strauss, and L. Patané, "Motor-skill learning in an insect inspired neuro-computational control system," *Front. Neurorobot.*, vol. 11, p. 12, Mar. 2017.
[53] J. H. Barron-Zambrano, C. Torres-Huitzil, and B. Girau, "Perception-driven adaptive CPG-based locomotion for hexapod robots," *Neurocomputing*, vol. 170, pp. 63–78, Dec. 2015.
[54] M. Akcakaya *et al.*, "Noninvasive brain–computer interfaces for augmentative and alternative communication," *IEEE Rev. Biomed. Eng.*, vol. 7, pp. 31–49, 2014.
[55] L. Minati, N. Yoshimura, and Y. Koike, "Hybrid control of a vision-guided robot arm by EOG, EMG, EEG biosignals and head movement acquired via a consumer-grade wearable device," *IEEE Access*, vol. 4, pp. 9528–9541, 2016.
[56] Y. Nakanishi *et al.*, "Mapping ECoG channel contributions to trajectory and muscle activity prediction in human sensorimotor cortex," *Sci. Rep.*, vol. 7, Mar. 2017, Art. no. 45486.

LUDOVICO MINATI (AM'00–M'04–SM'13) received the B.S. degree in information technology and computing and the M.S. degree in science from The Open University, Milton Keynes, U.K., in 2004 and 2006, respectively, the M.S. degree in applied cognitive neuroscience from the University of Westminster, London, U.K., in 2008, the B.S. degree in physical science and the M.S. degree in medical physics from The Open University in 2009, the Ph.D. degree in neuroscience from the Brighton and Sussex Medical School, U.K., in 2012, and the D.Sc. (doktor habilitowany) degree in physics from the Institute of Nuclear Physics – Polish Academy of Sciences, Krakow, Poland, in 2017.

He has held research and consulting roles across private companies and public institutions, including the Carlo Besta Neurological Institute, Milan, Italy, and the Brighton and Sussex Medical School, U.K. He has authored over 100 articles, and five inventions. He is currently specially appointed as an Associate Professor with the Institute of Innovative Research-Tokyo Institute of Technology, Japan, a Principal Specialist with the Complex Systems Theory Department, Institute of Nuclear Physics-Polish Academy of Sciences, a Guest Fellow with the Center for Mind/Brain Sciences, University of Trento, Italy, and a Freelance Consultant. His research interests include non-linear dynamical systems, chaotic oscillators, reconfigurable analog and digital computing, functional magnetic resonance imaging, advanced techniques for bio-signal analysis, brain machine/computer interfaces, and robotics.

Dr. Minati is also a Chartered Engineer and a member with the Institution of Engineering and Technology, U.K, a Chartered Physicist and a member with the Institute of Physics, London, U.K., and a Chartered Scientist and a member with the Institute of Physics and Engineering in Medicine, York, U.K. He is also a member with the Institute of Electronics, Information, and Communication Engineers, and the Japan Neuroscience Society.

MATTIA FRASCA (M'00–SM'09) received the degree in electronics engineering and the Ph.D. degree in electronics and automation engineering from the University of Catania, Italy, in 2000 and 2003, respectively, where he is currently an Associate Professor and teaches process control and systems theory.

His scientific interests include nonlinear systems and chaos, complex networks, and bio-inspired robotics. He has authored or co-authored six books and over 250 papers on refereed international journals and proceedings and is a co-author of two international patents.

Dr. Frasca is also the Associate Editor of the Int. J. Bi-furcations and Chaos, and the Editor of Chaos, Solitons and Fractals and served as the Associate Editor for the IEEE TRANSACTIONS ON CIRCUITS and SYSTEMS I from 2012 to 2015. He was one of the organizers of the 10th Experimental Chaos Conference, the Co-Chair of the 4th International Conference on Physics and Control and the Chair of the European Conference on Circuit Theory and Design 2017. He is a member of the Board of the Italian Society for Chaos and Complexity.

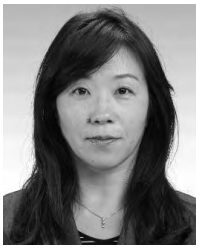

NATSUE YOSHIMURA received the M.S. degree from Tokyo Medical and Dental University, Japan, in 2006, and the Ph.D. degree from The University of Electro-communications, Japan, in 2009.

She was a Post-Doctoral Researcher with the Tokyo Institute of Technology from 2009 to 2010 and became an Assistant Professor. She has been an Associate Professor with the Institute of Innovative Research, Tokyo Institute of Technology, since 2015. She is currently a Visiting Researcher with the Integrative Brain Imaging Center, National Center of Neurology and Psychiatry. Her research interests include brain machine/computer inter-faces, brain activity information decoding relating to motor control, speech, and emotion, using noninvasive brain activity recording methods such as electroencephalography, and functional magnetic resonance imaging.

Dr. Yoshimura is a member of the Society for Neuroscience, the Japan Neuroscience Society, and the Japanese Society for Medical and Biological Engineering.

YASUHARU KOIKE received the B.S., M.S., and Ph.D. degrees in engineering from the Tokyo Institute of Technology, Tokyo, Japan in 1987, 1989, and 1996, respectively.

From 1989 to 1998, he was with Toyota Motor Corporation. From 1991 to 1994, he transferred to the Advanced Tele-communications Research Human Information Processing Laboratories, Kyoto, Japan. In 1998, he moved to the Precision and Intelligence Laboratory, Tokyo Institute of Technology, Tokyo, Japan, where he is currently a Professor with the Institute of Innovative Research. He was a Researcher of the Precursory Re-search for Embryonic Science and Technology, Japan Science and Technology Corporation, from 2000 to 2004 and of CREST, JST, from 2004 to 2014. His research interests include human motor control theory, human interface, and brain machine interface and their applications. He is a member of the Society for Neuroscience, the Institute of Electronics, Information and Communication Engineers, the Virtual Reality Society of Japan, and the Japan Neuroscience Society.